Multiple Notch ligands in the synchronization of the segmentation clock

Marcos Wappner,[1,2] Koichiro Uriu,[3,4] Andrew C. Oates,[5] and Luis G. Morelli[1,*]

[1]*Instituto de Investigación en Biomedicina de Buenos Aires (IBioBA) – CONICET/Partner Institute of the Max Planck Society, Polo Científico Tecnológico, Godoy Cruz 2390, Buenos Aires C1425FQD, Argentina*

[2]*Departamento de Física, FCEyN UBA, Ciudad Universitaria, 1428 Buenos Aires, Argentina*

[3]*School of Life Science and Technology, Institute of Science Tokyo, 2-12-1, Ookayama, Meguro-ku, Tokyo 152-8550, Japan*

[4]*Graduate School of Natural Science and Technology, Kanazawa University, Kakuma-machi, Kanazawa 920-1192, Japan*

[5]*Institute of Bioengineering, School of Life Sciences, Swiss Federal Institute of Technology Lausanne (EPFL), Lausanne 1015, Switzerland*

(Received 9 August 2024; accepted 4 September 2025; published 31 October 2025)

Notch signaling is a ubiquitous and versatile intercellular signaling system that drives collective behaviors and pattern formation in biological tissues. During embryonic development, Notch is involved in generation of collective biochemical oscillations that form the vertebrate body segments, and its failure results in embryonic defects. Notch ligands of the Delta family are key components of this collective rhythm, but it is unclear how different Delta ligands with distinct properties contribute to relaying information among cells. Motivated by the zebrafish segmentation clock, in this work we propose a theory describing interactions between biochemical oscillators, where Notch receptor is bound by both oscillatory and nonoscillatory Delta ligands. Based on previous *in vitro* binding studies, we first consider Notch activation by Delta dimers. This hypothesis is consistent with experimental observations in conditions of perturbed Notch signaling. Then we test an alternative hypothesis where Delta monomers directly bind and activate Notch and show that this second model can also describe the experimental observations. We next consider the effects of *cis*-inhibition in a model motivated by evidence from the mouse segmentation clock and find that this alternative is compatible with only part of the experimental data. We show how the dimer and monomer hypotheses assign different roles for a nonoscillatory ligand, as a binding partner or as a baseline signal. Finally, we discuss experiments to distinguish between the two scenarios. Broadly, this work highlights how a multiplicity of ligands may be harnessed by a signaling system to generate versatile responses.

DOI: 10.1103/7g6x-b238

I. INTRODUCTION

Intercellular signals coordinate cellular dynamics across tissues to generate collective behaviors and patterns [1–3]. A key signaling pathway is Notch, a versatile system controlling a wide variety of processes [4–7]. During embryonic development, Notch signaling coordinates cellular dynamics across tissues to generate patterns [3].

An attractive model system to study Notch signaling dynamics is the segmentation clock, a collective rhythm that governs the segmentation of the vertebrate body [8–11] [Fig. 1(a)]. This rhythm arises from a population of cellular genetic oscillators [12–20]. In zebrafish, cell autonomous oscillations of *her*/*hes* gene products are driven by a delayed negative feedback loop [21–26]. Additionally, oscillating *her* genes transcriptionally regulate the Notch ligand DeltaC, which also displays oscillating gene expression patterns [12]. The ligand binds Notch receptors in neighboring cells, resulting in the proteolytic cleavage and release of the Notch intracellular domain (NICD), which translocates to the nucleus and contributes to the activation of *her* genes in these neighboring cells [Fig. 1(b)]. This results in an oscillating signal, transferring the information of oscillation state from one cell to another.

It is thought that in this way, individual oscillators are synchronized by Notch signaling across the unsegmented tissue [Fig. 1(c)]. Zebrafish embryos with mutations in DeltaC or Notch1a, or which have been treated with the small molecule inhibitor DAPT to block Notch receptor cleavage [Fig. 1(b)], form a few normal segments and then start making defects [12,14,27–29]. The desynchronization hypothesis postulates that defective segments are caused by a loss of synchrony in the mutants [12] [Fig. 1(d)]. The clock starts in synchronized state [14,30], so a few normal segments can be formed before oscillators drift out of synchrony due to gene expression noise in the absence of intercellular coupling.

The mutant of DeltaD, another Notch ligand present in the zebrafish segmentation clock, also has a phenotype consistent with the desynchronization hypothesis [15]. However, although DeltaD shows some refinement of gene expression stripes in the anterior PSM, it does not display oscillatory patterns of mRNA [31–33] or protein [34,35] in the posterior PSM or tailbud and is not known to be regulated by Her proteins [36]. It is intriguing that such a constant DeltaD signal, without rhythmic temporal information, has a similar effect on synchronization.

*Contact author: morelli.luis.g@gmail.com

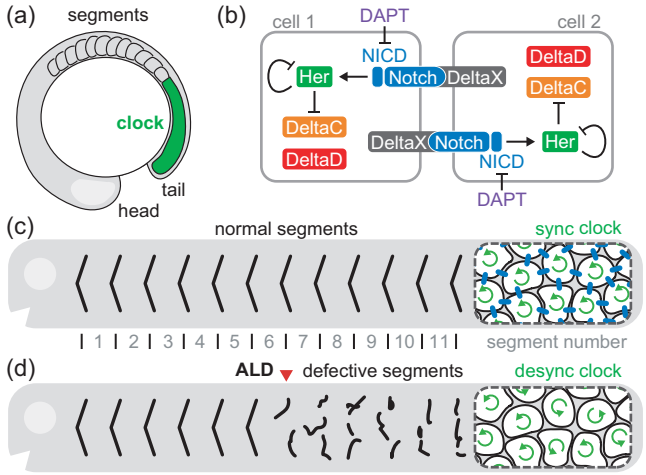

FIG. 1. (a) Schematic representation of zebrafish embryonic segmentation showing the unsegmented clock tissue (green) and forming segments. (b) Delta-Notch intercellular coupling synchronizes individual oscillators. [(c) and (d)] Schematic zebrafish showing (c) normal segment boundaries (black lines) and (d) defective boundaries (broken black lines). Red arrowhead indicates the onset of defective segments [anterior limit of defects (ALD), see text]. Magnifications of the tail tip show (c) synchronized individual oscillators (coherent circular arrows) in the presence of coupling (blue bars) and (d) desynchronized oscillators (incoherent circular arrows) in its absence.

It has been shown that DeltaC and DeltaD colocalize *in vivo*, and both ligands associate *in vitro* forming heterodimers and homodimers [34]. Thus, it is possible that DeltaC and DeltaD form dimers *in vivo* as well, and it is these dimers that can bind and activate the Notch receptors in neighboring cells. Additionally, immunoprecipitation experiments show that heterodimers form in larger quantities than homodimers, suggesting the affinity is larger for the former than for the latter. With this hypothesis, the role of DeltaD would be to provide a necessary binding partner for DeltaC [34].

Previous theoretical work addressed diverse aspects of Notch signaling in the segmentation clock. Phase theories that coarse-grain the molecular details of oscillator coupling have been successfully used to study mean-field synchronization dynamics [14], the effects of coupling delays on spatiotemporal dynamics [37–39], the impact of oscillator mobility [40,41], perturbations [42], asymmetric pulsed coupling [43,44], and Notch signaling modes [45,46]. Other generic theories consider the possibility that the collective rhythm arises from Notch-driven excitable oscillators [47–49]. Further work included molecular aspects of Notch signaling, for example, to demonstrate synchronized biochemical oscillations [22,50–52], to study Notch receptor modulation [53], amplitude death by coupling delays [18], the effects of noise and cell divisions [13], to describe kinematic gene expression waves [54,55], and to reveal the effects of noisy communication channels [46]. Finally, the different ways to coarse-grain the details of these molecular aspects have consequences on the dynamic modes accessible to the system [56]. This coupling coarse-graining was used to study the effects of delayed coupling, relating dynamic modes to experimental findings [18]. While these previous studies shed light on different aspects of Notch signaling in the segmentation clock, they did not consider distinct roles of ligands.

In this work, we formulate a theory of Delta-Notch coupling in the zebrafish segmentation clock based on existing experimental evidence. We use a mean-field approach to study synchronization under different scenarios to investigate the role of the ligand DeltaD. We first explore the hypothesis that binding of Delta dimers to Notch receptors mediates synchronization. We show the roles of different dimers in accounting for different aspects of experimental data. We then formulate a monomer binding theory and show how it may also explain the role of DeltaD. In contrast, a theory including additional *cis* interactions that endows DeltaD with a distinct role is not consistent with all experimental evidence. We finish with two competing hypotheses and discuss their predictions, suggesting experiments that may be able to distinguish among them.

II. OSCILLATOR AND SIGNAL RECEPTION

In the zebrafish segmentation clock, genes of the *her/hes* family have binding sites for their own products that can act as transcriptional repressors [8]. It has been proposed that genetic oscillations occur as a consequence of delayed inhibition of these *her* genes [22–25,32,57–59]. It is thought that a network of *her* family protein dimers constitutes the core oscillator [25,26]. Here we focus on the roles of the coupling network components, so we take a parsimonious approach in the description of this core oscillator. A single variable $h_i(t)$ stands for the protein concentration of a generic *her* gene in cell i, with $i = 1, \ldots, N_c$ and N_c the total number of cells. The core oscillator dynamics is

$$\dot{h}_i = -h_i + \beta_H \underbrace{\frac{1}{1+[h_i(t-\tau_i)]^\eta}}_{f_-(h_i(t-\tau_i))} \underbrace{\frac{1+\alpha[\sigma s_i(t-\tau_i)]^\eta}{1+[\sigma s_i(t-\tau_i)]^\eta}}_{f_+(s_i(t-\tau_i))}. \quad (1)$$

The first term describes protein degradation, with unit rate since we set the inverse degradation rate of Her proteins as the timescale to render the system dimensionless (Appendix A). The second term describes protein synthesis, with dimensionless basal synthesis rate β_H. Synthesis is modulated by a regulatory function, with a negative feedback f_- resulting from autoinhibition [23,24], and a positive regulation f_+ describing the effect of integrated signals $s_i(t)$ from other cells. Delayed synthesis regulation accounts for the fact that synthesis rate at time t depends on the concentration of regulatory factors at time $t - \tau_i$, where τ_i is the time it takes to produce the Her protein in cell i. The values of these synthesis delays are sampled from a normal distribution to capture the effect of gene expression noise [60] (Appendix A). Since the period of oscillations is determined to first order by the synthesis delay [22,60,61], with this variability in the delays we introduce a variability in the period of individual oscillators. The intensity of the activation α is the fold change in synthesis rate caused by signals s_i. The dimensionless concentration scale σ sets a threshold for signal-driven synthesis activation. The analogous concentration scale for the binding of Her proteins in f_- is used as a concentration scale for the variables. The Hill exponent η is an effective nonlinearity accounting for

TABLE I. Parameter table used in synchronization maps in the main text. DC and DD denote DeltaC and DeltaD. H.e. denotes Hill exponent. C.V. is the coefficient of variation.

Parameter	Dimers	Monomers	Description
δ_C	1	1	DC degradation rate
δ_D	1	1	DD degradation rate
δ_E	1	1	DC:DD degradation rate
δ_F	1	1	DC:DC degradation rate
δ_G	1	1	DD:DD degradation rate
δ_N	1	1	Notch degradation rate
δ_S	1	1	NICD degradation rate
β_H	28	28	Her synthesis rate
β_C	26	39	DC synthesis rate
β_D	17	20	DD synthesis rate
β_N	24	30	Notch synthesis rate
λ_{E+}	1	–	DC:DD dimerization rate
λ_{E-}	0.1	–	DC:DD dissociation rate
λ_{F+}	0.1	–	DC:DC dimerization rate
λ_{F-}	0.1	–	DC:DC dissociation rate
λ_{G+}	0.1	–	DD:DD dimerization rate
λ_{G-}	0.1	–	DD:DD dissociation rate
κ_C	–	0.02	DC binding rate to Notch
κ_D	–	0.01	DD binding rate to Notch
κ_E	0.2	–	DC:DD binding rate to Notch
κ_F	0.02	–	DC:DC binding rate to Notch
κ_G	0.009	–	DD:DD binding rate to Notch
σ	0.1	0.1	Signal activation threshold
γ	1	1	DC inhibition threshold
η_H	2.5	7	Her self-inhibition H.e.
η_S	2.5	7	Her activation by signal H.e.
η_C	2.5	7	DC inhibition by Her H.e.
α	10	10	Fold change in synthesis rate
τ_H	4.2	4.2	Mean Her synthesis delay
σ_τ/τ_H	0.03	0.03	C.V. of Her synthesis delay
τ_C/τ_H	1.7	1.7	Relative DC synthesis delay

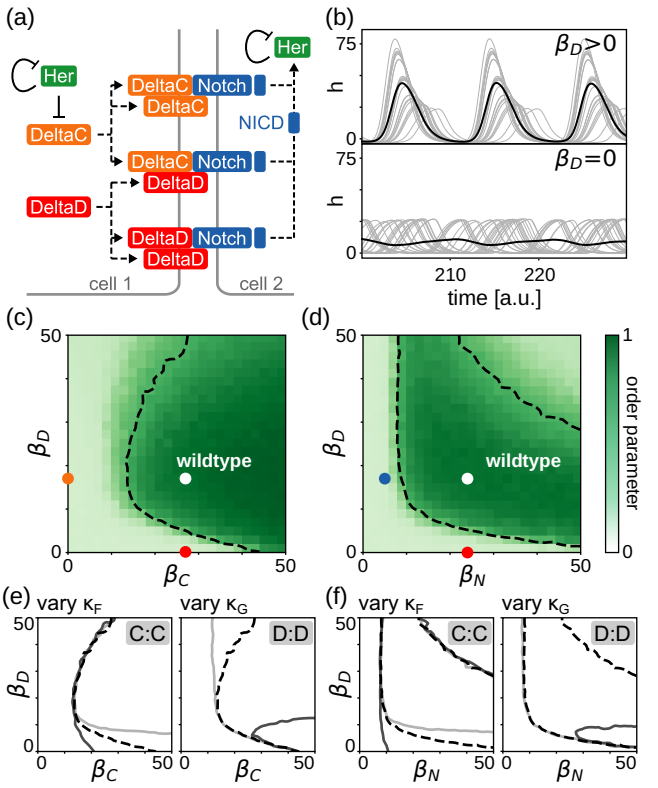

FIG. 2. Dimer binding hypothesis is compatible with desynchronization phenotypes in steady state. (a) All dimers from DeltaC and DeltaD form and can bind and activate Notch. (b) Steady-state individual oscillations $h_i(t)$ (gray lines, 25 of 100 are displayed) and mean-field $\bar{h}(t)$ (black line) for $\beta_D > 0$ (top) and $\beta_D = 0$ (bottom). [(c) and (d)] Steady-state order parameter $\bar{R}$ in terms of (c) DeltaC and DeltaD synthesis rates, and (d) Notch and DeltaD synthesis rates. Dashed line indicates the boundary of the sync region, defined by $\bar{R} = R_T = 0.6$. Dots indicate wildtype parameters (white), and mutants for DeltaC (orange), DeltaD (red), and Notch (blue). Parameter values for these conditions are determined below from desynchronization dynamics in Fig. 3. [(e) and (f)] Changes to the sync region boundary in terms of (e) DeltaC and DeltaD synthesis rates, and (f) Notch and DeltaD synthesis rates, caused by varying Notch binding rates. Left: Varying C:C Notch binding rate, $\kappa_F = 0.002$ (light), 0.02 (dashed black), and 0.2 (dark). Right: Varying D:D Notch binding rate, $\kappa_G = 0.002$ (light), 0.009 (dashed black), and 0.2 (dark). Dashed black lines are the same as in (c) and (d). [(c)–(f)] are 25×25 pixels, averaged over 10 independent realizations. Wildtype parameter values in Table I.

intermediate molecular interactions. The particular form of the regulatory function in Eq. (1) results from assuming that binding of Her proteins and the NICD to the promoter of the *her* gene occurs independently (Appendix A).

Communication between cells occurs through the binding of ligands from other cells to Notch receptors, eliciting the NICD signal in the receiving cell. The dynamics of signal s_i and Notch receptor concentration n_i are given by

$$\dot{s}_i = -\delta_S s_i + K n_i, \tag{2}$$

$$\dot{n}_i = -\delta_N n_i + \beta_N - K n_i, \tag{3}$$

where δ_S and δ_N are the dimensionless decay rates of the signal and receptor, respectively, and β_N is the Notch synthesis rate. The second term in Eq. (2) describes signal production due to the binding of ligands to Notch receptors, with K a total ligand binding activity. Next, we specify contributions of different Notch ligands to K.

III. NOTCH SIGNALING ACTIVATED BY DIMERS

Following the proposal that DeltaC and DeltaD form dimers [34] [Fig. 2(a)], the monomer concentrations $c_i(t)$ and $d_i(t)$ follow

$$\dot{c}_i = -\delta_C c_i + \beta_C \frac{1}{1 + [\gamma h_i(t - \tau_C)]^{\eta_c}} + \lambda_E^- e_i - \lambda_E^+ c_i d_i + \lambda_F^- f_i - \lambda_F^+ c_i^2, \tag{4}$$

$$\dot{d}_i = -\delta_D d_i + \beta_D + \lambda_E^- e_i - \lambda_E^+ c_i d_i + \lambda_G^- g_i - \lambda_G^+ d_i^2, \tag{5}$$

including terms describing degradation with rates δ_C and δ_D and terms describing synthesis with basal rates β_C and β_D. We include a modulation of the synthesis rate of DeltaC by the oscillator, since DeltaC promoter contains binding sites for *her* products [25] and mRNA patterns show signatures of oscillatory expression [32]. The concentration of Her in this modulation is evaluated at the past time $t - \tau_C$ to account for the time required to produce DeltaC molecules. The dimensionless concentration scale γ is the threshold for the onset of *deltaC* promoter repression by Her, and Hill exponent η_c is the effective nonlinearity of this repression. DeltaD is not known to be transcriptionally regulated by Her during somitogenesis and its mRNA patterns do not display signatures of oscillation [32], so we do not include a modulation of DeltaD synthesis. Additional terms describe dimerization, where variables $e_i(t)$, $f_i(t)$, and $g_i(t)$ describe the concentrations of DeltaC:DeltaD, DeltaC:DeltaC, and DeltaD:DeltaD dimers, respectively, and $\lambda_E^{\pm}$, $\lambda_F^{\pm}$, and $\lambda_G^{\pm}$ are association (+) and dissociation (−) rates. The variables $c_i(t)$ and $d_i(t)$ refer to concentrations of mature ligands, after completion of endocytic trafficking and post-translational modifications required for enhanced activity [62].

Dimer dynamics are

$$\dot{e}_i = -\delta_E e_i + \lambda_E^+ c_i d_i - \lambda_E^- e_i - \kappa_E e_i \bar{n}, \tag{6}$$

$$\dot{f}_i = -\delta_F f_i - \lambda_F^- f_i + \lambda_F^+ c_i^2 - \kappa_F f_i \bar{n}, \tag{7}$$

$$\dot{g}_i = -\delta_G g_i - \lambda_G^- g_i + \lambda_G^+ d_i^2 - \kappa_G g_i \bar{n}, \tag{8}$$

resulting in total ligand binding activity

$$K = \kappa_E \bar{e} + \kappa_F \bar{f} + \kappa_G \bar{g}, \tag{9}$$

where δ_E, δ_F, and δ_G are dimer degradation rates and κ_E, κ_F, and κ_G are the binding rates of dimers to Notch receptors. The bar notation $\bar{x}$ represents the average concentration of species x over all cells that interact with cell i. This average results from the assumption that the cell surface available for signaling is shared equally among all neighbors (Appendix A).

In this work we describe synchronization dynamics in the posterior tip of the elongating body axis, the so-called tailbud, which is a relatively homogeneous region of the tissue oscillating in synchrony [63]. Cell mixing is prevalent within this region [64–66], and theory has shown that mixing causes an effective mean-field regime [41,67] that enhances synchronization [40,65]. Thus, in this work we consider a mean-field description of the tail, where all N_c cells interact with every other cell, so

$$\bar{x} = \frac{1}{N_c} \sum_{i=1}^{N_c} x_i. \tag{10}$$

Together with Eqs. (1)–(3), Eqs. (4)–(9) and the mean-field assumption (10) complete the model. All equations, variables and parameters are dimensionless (Appendix B). In this model, negative feedback-induced autonomous oscillation of Her directly drives the oscillation of DeltaC [Eqs. (1) and (4)]. This in turn may translate into an oscillation of some dimers [Eqs. (6) and (7)], causing the ligand binding activity K to oscillate [Eq. (9)]. Oscillatory binding activity drives an oscillatory signal in contacting cells [Eqs. (3) and (2)], which ends up modulating the Her regulatory function [Eq. (1)]. In this way, the oscillatory state of one cell is communicated to other cells.

IV. STEADY-STATE SYNCHRONIZATION MAPS

We set parameter values following constraints from experimental observations and theoretical considerations which result in synchronized oscillations [Fig. 2(b) (top), Appendix C and Fig. S1(a)] [68]. Next, we seek to describe loss of synchrony as observed in phenotypes of mutant conditions [12]. Mutant conditions of signaling components, as well as other perturbations, can be described in the model by altering the corresponding synthesis rates β_C, β_D, and β_N. For instance, the DeltaD mutant could be described by setting $\beta_D = 0$. We find that synchronization is lost in this condition, matching the experimental evidence for desynchronization [15], even though DeltaD is not regulated by the oscillator [Fig. 2(b) (bottom)]. To quantify how different perturbations may affect the collective rhythm, we introduce a synchronization index, the Kuramoto order parameter R (Appendix F) [69], taking values between 0 (desynchronized) and 1 (synchronized). We construct steady-state synchronization maps that show the stationary value of this order parameter after transients have elapsed [Figs. 2(c) and 2(d)]. In these maps, we can introduce synchronization boundaries that separate synchronized from desynchronized states by setting a threshold R_T on the value of the order parameter. Dashed lines in Figs. 2(c) and 2(d) indicate this boundary with the choice $R_T = 0.6$. The presence of segmentation defects in mutant phenotypes for the Delta ligands and the Notch receptor are interpreted as desynchronized states in these maps. We can see that it is possible to choose a wildtype parameter set within the synchronized region, such that reducing the synthesis rates of the coupling components, will result in drastic loss of steady-state synchrony [dots in Figs. 2(c) and 2(d)]. In such parametrization of the wildtype, all coupling components are required for steady-state synchronization, in agreement with mutant phenotypes for the ligands and the receptor [15]. In particular, this result is consistent with a role for DeltaD in the synchronization of the segmentation clock. Furthermore, we observe that starting from the $\beta_D = 0$ condition and increasing either β_C or β_N we can move back into the synchronized region, see red dot in Figs. S2(a) and S2(b) [68]. This predicts a rescue of DeltaD mutant defects with adequate DeltaC or Notch overexpression.

These maps also predict a nonmonotonic behavior of the order parameter with DeltaD synthesis rate β_D [Figs. 2(c) and 2(d)]. Extended synchronization maps show that for large β_D synchrony is lost, suggesting that nonoscillating components become so abundant that they titrate out the rhythmic DeltaC signal [Fig. S2(a) and S2(b)] [68]. This is consistent with experiments, where DeltaD overexpression by injection of high mRNA levels caused defective segments [70], likely due to loss of synchrony. In contrast, transgenic zebrafish expressing 50 times the level of wildtype DeltaD, driven by the endogenous regulatory regions, did not cause desynchronization phenotypes [35]. The mRNA injection experiments [70] likely produced larger DeltaD protein levels than the transgenic line [35]. However, it is not straightforward to quantitatively

compare these two different experiments, where overexpression results either from translation of mRNA injected at an early developmental stage—which causes a widespread ectopic expression—or from transcription of additional copies under the control of the endogenous regulatory DNA in the case of the transgenic animal. In addition, since the protein concentration $d_i(t)$ refers to the mature, active ligand concentration [62], the 50-fold increase in protein levels in the transgenic zebrafish does not straightforwardly translate into a 50-fold increase in the value of β_D in the theory. Thus, we do not attempt a quantitative description of the transgenic overexpression result here. Still, it is interesting to test whether the model can qualitatively account for DeltaD overexpression data, so we look for parameters that control the shape of the synchronization region for large values of β_D. Boundaries of steady-state synchronization regions can be tuned by parameters that control aspects of dimer kinetics [Figs. 2(e) and 2(f) and Fig. S3] [68]. For example, increasing the value of κ_F changes the point on the $\beta_D = 0$ axis where increasing the values of β_C or β_N leads to a synchronization transition [left panels in Figs. 2(e) and 2(f)]. In contrast, the boundary for large β_D can be shaped by the value of κ_G, without significantly changing the synchronization transition at $\beta_D = 0$. Thus, DeltaD overexpression can be captured in the model while preserving the behavior of the DeltaD mutant condition. Taken together, these data suggest that the wildtype is placed in a region of the synchronization map with some room for larger DeltaD concentrations before synchrony is lost.

V. DESYNCHRONIZATION DYNAMICS

In the embryo, the segmentation clock is initiated in a synchronized state [14,30]. It is thought that in Notch signaling mutants, impaired coupling leads to desynchronization of the collective rhythm and eventually causes the observed defective segments [12–15]. Although all mutants of coupling components end up desynchronized, some start making defects earlier than others [33]. These differences in the onset of defects is often quantified as the anterior limit of defects (ALD) [32]. While the *deltaC* mutant has a mean ALD of about 5.5 [27,29], *deltaD* and *notch1a* have a mean ALD of 8 [14,27,35]. There are multiple *notch* genes expressed in the segmentation clock [71], but segmentation phenotypes have not been reported for *notch* mutants other than *notch1a*. This may reflect that the individual contributions from each of the other Notch receptors to synchronization is small. This interpretation is consistent with the identical ALD of the *deltaC* mutant and the DAPT assay [14], which should block the cleavage of all Notch receptors.

The differences in ALD can be interpreted as a consequence of different desynchronization rates in the mutant backgrounds. To test this aspect of mutant phenotypes, we introduce a computational desynchronization assay. Experimental observations show that *her7* oscillations start synchronized and make a few cycles before the initiation of somitogenesis [14]. Similarly, a Her1 protein reporter shows several synchronized cycles at the segmentation clock onset [30]. With this motivation, we set the initial values of all variables to zero for all cells. Simulations show that oscillations start synchronized and synchrony decays in the absence of key

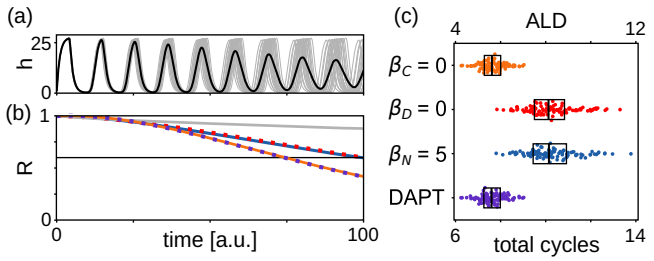

FIG. 3. Dimer binding hypothesis is compatible with transient desynchronization phenotypes. (a) Individual oscillators $h_i(t)$ (gray lines, 20 of 100 are displayed) and mean-field $\bar{h}(t)$ (black line) for $\beta_C = 0$. (b) Order parameter as a function of time from initially synchronized state for different conditions: wildtype parameters (gray line), $\beta_C = 0$ (orange line), $\beta_D = 0$ (dotted red line), $\beta_N = 5$ (blue line), and DAPT treatment (dotted purple line). Horizontal light gray line marks the threshold value $R_T = 0.6$ of the order parameter. (c) Onset of defective segments for different conditions as indicated. Top axis is ALD in cycles from the onset of segmentation, bottom axis is cycles from the onset of oscillations (Appendix F). Dots are 100 individual realizations, with 100 cells each. Bars are medians and boxes display the interquartile range.

coupling components [Fig. 3(a)]. We then look for parameter values β_C, β_D, and β_N that capture experimental observations of ALD in mutant backgrounds, while keeping the rest of parameters as in Fig. 2 (Appendix C). In the theory, the onset of defects can be associated with the threshold value R_T for the Kuramoto order parameter. We interpret that below this value, synchrony is not enough to produce a normal segment boundary. We obtain a parameter set for which the desynchronization assay is consistent with ALD measurements of different conditions: the wildtype stays synchronized, threshold crossing occurs soonest for the DeltaC mutant condition, and at later similar times for the DeltaD and Notch mutant conditions [Fig. 3(b)]. Synchrony decay for DeltaC mutant occurs as fast as in a simulation of saturated DAPT treatment (Appendix A) [13,14]. Scaling the time by the cycle duration we can construct ALD plots (Appendix F), which show good agreement with experimental observations [Fig. 3(c)].

VI. THE ROLE OF DIFFERENT DIMERS

Next, we ask how different dimers contribute to shaping the synchronization region by alternatively setting to zero their association and dissociation rates together with their Notch binding rates. The DeltaC:DeltaD heterodimer is important to generate a wide synchronization region, with a broad range of β_C values where the DeltaD mutant would result in loss of synchronization [Fig. 4(a)]. The DeltaC:DeltaC homodimer further enables synchronization in the low DeltaD region, such that large β_C could rescue the DeltaD mutant [Fig. 4(b)]. In contrast, the DeltaD:DeltaD homodimer can inhibit synchronization for large DeltaD concentrations [Fig. 4(c)]. Excluding both homodimers results in a symmetric synchronization map, in which loss of any ligand is equivalent [Fig. 4(d)]. This synchronization map with the heterodimer only is consistent with the steady-state properties of mutants, that is, loss of synchrony. However, the numerical desynchronization assay displays the same ALD for DeltaC and DeltaD

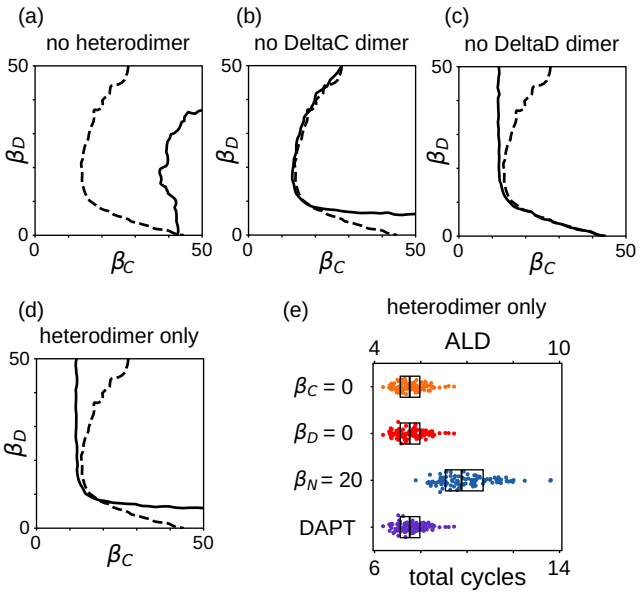

FIG. 4. Individual dimers influence distinct regions of the synchronization map. [(a)–(d)] Changes to sync region boundary in Fig. 2(c) (dashed line) for (a) $\lambda_E^{\pm} = 0$ and $\kappa_E = 0$ (solid line), (b) $\lambda_F^{\pm} = 0$ and $\kappa_F = 0$ (solid line), (c) $\lambda_G^{\pm} = 0$ and $\kappa_G = 0$ (solid line), (d) $\lambda_F^{\pm} = \lambda_G^{\pm} = 0$ and $\kappa_F = \kappa_G = 0$ (solid line). (e) Onset of defective segments for different conditions as indicated. Axes, dots, and boxes as in Fig. 3(c). Dashed line, number of realizations and other parameters as in Figs. 2(e) and 2(f).

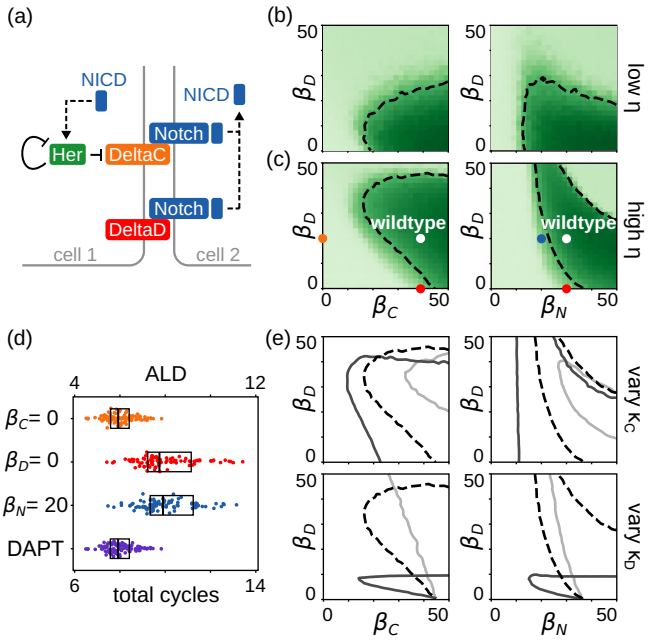

FIG. 5. Monomer binding hypothesis is compatible with experimental data. (a) DeltaC and DeltaD monomers can bind and activate Notch. [(b) and (c)] Steady-state order parameter $\bar{R}$ for (b) effective nonlinearity $\eta = 2.5$ and (c) $\eta = 7$, in terms of (left) DeltaC and DeltaD synthesis rates, and (right) Notch and DeltaD synthesis rates. Dashed line, dots, color scale, and number of realizations as in Figs. 2(c) and 2(d). Wildtype parameter values in Table I. (d) Onset of defective segments for different conditions as indicated. Axes, dots, and boxes as in Fig. 3(c). (e) Changes to the sync region boundary in terms of (left) DeltaC and DeltaD synthesis rates, and (right) Notch and DeltaD synthesis rates, caused by varying Notch binding rates. Top: $\kappa_C = 0.01$ (light), 0.03 (dashed black), and 0.3 (dark). Bottom: $\kappa_D = 0.002$ (light), 0.01 (dashed black), and 0.3 (dark). Dashed black lines are the same as in (c). Number of realizations as in Figs. 2(e) and 2(f).

mutants, failing to recapitulate distinct embryonic mutant phenotypes [Fig. 4(e)].

In summary, the hypothesis that DeltaC and DeltaD dimers bind and activate the Notch receptor seems to be consistent with key experimental observations of mutant phenotypes [Figs. 2 and 3]. In this hypothesis, the role of DeltaD is to provide a binding partner for DeltaC. So even though DeltaD is not transcriptionally regulated, through its interaction with DeltaC it cooperates in generating an oscillatory signal. Thus, the heterodimer DeltaC:DeltaD seems to be the key player [Fig. 4(a)], and homodimers introduce an asymmetry that explains the observed differences in the desynchronization assays of DeltaC and DeltaD mutants [Figs. 3(c) and 4(e)].

VII. NOTCH SIGNALING ACTIVATED BY MONOMERS

In the most common view of Notch signaling, ligands are pictured to bind receptors as monomers [72,73]. Activation of the Notch receptor by Delta dimers would be a paradigm shift in this view [34,74]. Thus, we wanted to test whether dimerization is necessary to explain the data or whether monomer binding of the Notch receptor is able to reproduce experimental observations as well. We formulated an alternative theory, in which single DeltaC and DeltaD proteins can bind Notch receptors as monomers, eliciting a signal in the receiving cell [Fig. 5(a)]. Without dimerization, the dynamics of DeltaC and DeltaD concentrations are

$$\dot{c}_i = -\delta_C c_i + \beta_C \frac{1}{1 + [\gamma\, h_i(t - \tau_C)]^{\eta}} - \kappa_C c_i \bar{n}, \tag{11}$$

$$\dot{d}_i = -\delta_D d_i + \beta_D - \kappa_D d_i \bar{n}. \tag{12}$$

The degradation and synthesis terms are the same as in previous Eqs. (4) and (5), but instead of dimer association and dissociation terms we now include loss terms due to direct binding of the monomer ligands to Notch receptors, with binding rates κ_C and κ_D. The resulting ligand binding activity $K(t)$ now has contributions from DeltaC and DeltaD ligands,

$$K = \kappa_C \bar{c} + \kappa_D \bar{d}, \tag{13}$$

where $\bar{c}$ and $\bar{d}$ are DeltaC and DeltaD mean fields [Eq. (10)]. Together, Eqs. (1)–(3) and (11)–(13) formalize the hypothesis where DeltaC and DeltaD ligands bind and activate the Notch receptor.

Synchronized oscillations are also possible through monomer binding [Fig. S1(b)] [68]. We performed a search in parameter space to establish whether this scenario could be compatible with experimental data. We found that with a parametrization similar to the dimer scenario, synchronization maps do not have a prominent region where synchronization is lost by removing DeltaD [Fig. 5(b)]. However, we found that increasing the effective nonlinearity η in the regulatory function, steady-state synchronization maps are consistent with the phenotypes of DeltaC, DeltaD, and Notch mutants

[12,15] [Fig. 5(c) and Fig. S4] [68]. In particular, there is a broad region in the synchronization map where loss of DeltaD causes desynchronization [Fig. 5(c) and Figs. S2(c) and S2(d)] [68]. Furthermore, the desynchronization assay shows that this hypothesis is also compatible with the different desynchronization rates observed in mutants [Fig. 5(d)].

For small values of β_D where synchronization is lost, increasing the values of β_C and β_N can bring the system to a synchronization transition and synchrony recovery. These maps also reveal that for large values of β_D synchronization is lost [Figs. 5(b) and 5(c)]. However, the boundary of synchronization regions is controlled by the Notch binding rates κ_C and κ_D [Fig. 5(e)]. Decreasing κ_D extends the synchronization region towards larger β_D values, so synchrony may be preserved under strong DeltaD overexpression [35]. Increasing κ_C generally shifts the synchronization region towards smaller values of the syntheses rates, so strong binding of DeltaC to Notch may reduce the cost of sustaining synchrony in terms of molecular turnover.

VIII. *CIS*-INHIBITION CAN SYNCHRONIZE OSCILLATIONS

It has been proposed that *cis* interactions of Notch ligands with the receptor can happen in different contexts and species [75]. This means that, besides binding receptors in neighboring cells, ligands can bind receptors within the same cell. Although we know of no evidence for *cis* interactions in the zebrafish segmentation clock, evidence from mammals prompted us to consider this possibility.

In the mouse, the divergent Notch ligand Delta-like 3 (DLL3) is thought to bind Notch exclusively in *cis* [76], and to reside almost entirely in the Golgi [77], sequestering the receptor inside cells and in this way inhibiting the signal reception [78]. While this ligand is constantly expressed, it has been proposed to play a role in the modulation of cyclic Notch availability, contributing to segmentation clock collective oscillations [78]. The zebrafish ligand DeltaC has been proposed to be orthologous to DLL3 [79–81]. Along this line, DeltaC intracellular puncta observed in the antibody staining of the anterior PSM [34] could be interpreted as evidence for *cis* interactions.

In the mouse segmentation clock, oscillatory Delta-like 1 (DLL1) is coexpressed with DLL3 [82,83]. In contrast to DLL3, DLL1 can bind Notch receptors both in *cis* and in *trans*, respectively inhibiting or activating the signaling pathway [78]. An *in vitro* assay with rat DLL1 using mammalian derived cell lines combined with theoretical modeling revealed how this dual role enables mutually exclusive signaling states [84,85]. Similarly, in zebrafish embryonic neural tissue, DeltaD was shown to play a dual role in lateral inhibition, both as a *trans*-activator and *cis*-inhibitor of Notch [86].

Considering this evidence, here we introduce a model where both DeltaC and DeltaD *cis*-inhibit Notch receptors in the same cell, and only DeltaD *trans*-activates Notch receptors in neighboring cells [Fig. 6(a)]. In the model, this is formalized setting $\kappa_C = 0$ (no *trans*-activation) and including the loss terms $-\kappa_C^{\rm cis} c_i n_i$ in Eqs. (3) and (11), and $-\kappa_D^{\rm cis} d_i n_i$ in Eqs. (3) and (12), where $\kappa_C^{\rm cis}$ and $\kappa_D^{\rm cis}$ are the dimensionless binding rates of DeltaC and DeltaD to Notch in *cis* (Appendix D). In contrast to the mouse segmentation clock model [78], here the *trans*-activator is not transcriptionally regulated by the oscillator. Still, in the presence of these interactions, we find that steady-state synchronization maps display a robust synchronization region and are compatible with the different mutant conditions in steady state [Fig. 6(b)].

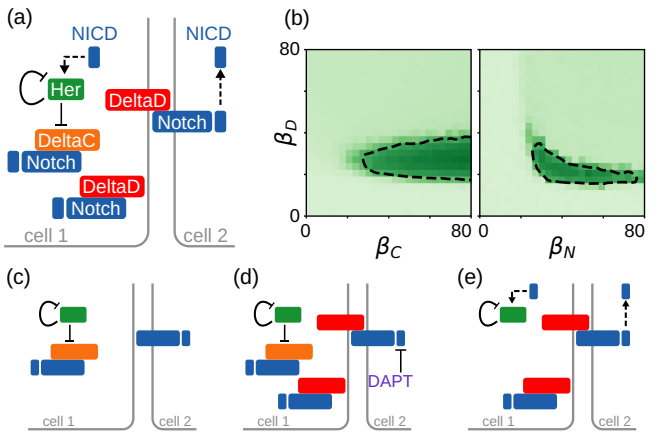

FIG. 6. A *cis*-interaction model can synchronize oscillations. (a) DeltaD and DeltaC inhibit Notch in *cis*, DeltaD also activates Notch in *trans*. (b) Steady-state order parameter $\bar{R}$ in terms of (left) DeltaC and DeltaD synthesis rates and (right) Notch and DeltaD synthesis rates. Dashed line, color scale, and number of realizations as in Figs. 2(c) and 2(d). Parameter values as in Table I, except for $\sigma = 0.5$ and $\kappa_C = 0$, with $\kappa_C^{\rm cis} = 0.3$ and $\kappa_D^{\rm cis} = 0.1$ motivated by measurements in Ref. [84]. [(c)–(e)] Perturbations of the circuit diagram in (a) corresponding to (c) DeltaD mutant, (d) treatment with DAPT, and (e) DeltaC mutant.

This model endows DeltaD with a third, distinct role in synchronization. The oscillator cyclically inhibits DeltaC, which binds Notch in *cis*, periodically sequestering the receptor in direct competition with DeltaD. As a consequence, levels of free DeltaD also oscillate, producing cyclical activation of Notch receptors in neighboring cells. In this way, DeltaD carries the oscillatory signal between neighboring oscillators through an indirect interaction with oscillatory DeltaC.

While this model captures the steady-state mutant phenotypes, the distinct features revealed by desynchronization assays cannot be reproduced by including *cis*-inhibition [Fig. S5] [68]. Loss of DeltaD in the model is equivalent to loss of DeltaC or to signal blocking by DAPT, while in the embryo it produces slower desynchronization. This is because without DeltaD, there is no ligand to activate receptors in neighboring cells [Fig. 6(c)]. This is an equivalent loss of signal to DAPT inhibition of Notch, where DeltaD binds Notch receptors but the NICD cannot be released [Fig. 6(d)]. Finally, loss of DeltaC decouples the signaling components from the oscillator and, while DeltaD still binds Notch receptors, it can only transmit a constant signal [Fig. 6(e)]. Thus, although this model assigns an interesting new role for DeltaD in synchronization, in the following sections we continue only with the analysis of the hypotheses that can capture the desynchronization phenotypes as well.

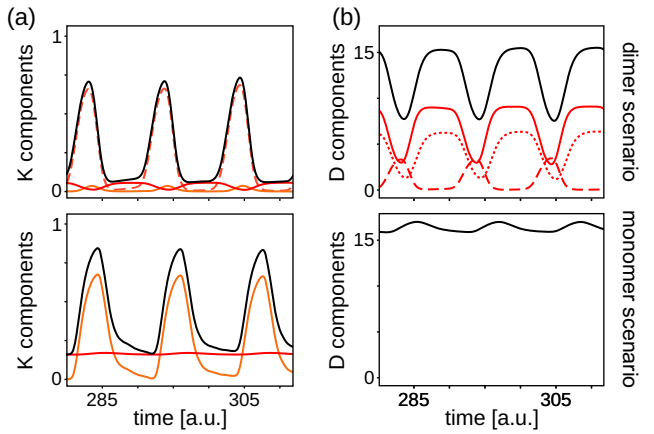

FIG. 7. Comparison of dimer and monomer scenarios. (a) Decomposition of contributions to the total ligand binding activity $K(t)$ (solid black line). Top: Dimers binding activity $\kappa_F f(t)$ (orange line), $\kappa_G g(t)$ (solid red line), and $\kappa_E e(t)$ (dashed red line). Bottom: Monomers binding activity $\kappa_C c(t)$ (orange line) and $\kappa_D d(t)$ (red line). (b) Decomposition of contributions to the total DeltaD dimensionless concentration $d_T(t)$ (solid black line). Top: $d(t)$ (solid red line), $e(t)$ (dashed red line), and $g(t)$ (dotted red line) in the dimer scenario. Bottom: $d(t) = d_T(t)$ in the monomer scenario.

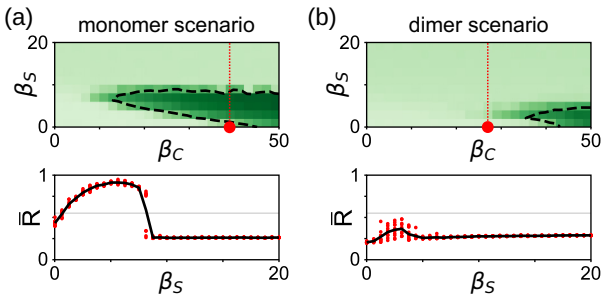

FIG. 8. NICD overexpression assay in DeltaD mutant predicts distinct outcomes for monomer and dimer scenarios. Top: Steady-state order parameter $\bar{R}$ in terms of DeltaC and NICD synthesis rates for the (a) monomer and (b) dimer scenarios. Red dot is the DeltaD mutant condition for $\beta_S = 0$ and vertical red dotted line indicates the cut plotted in bottom panels. Dashed line, color scale, and number of realizations as in Figs. 2(c) and 2(d). Bottom: Steady-state order parameter $\bar{R}$ as a function of β_S along the red dotted line in top panels for (a) monomer and (b) dimer scenarios. Red dots are 10 independent realizations and black line is the average. Horizontal gray line indicates the threshold R_T. Parameters as in corresponding scenario, except for $\beta_D = 0$ (Table I).

IX. DeltaD ROLE AND DYNAMICS

Going back to our initial motivation, how does an unregulated DeltaD signal, *a priori* without rhythmic temporal information, contribute to synchronization? To address this question, we consider the contributions to the ligand binding activity $K(t)$ [Fig. 7(a)]. We have shown two scenarios that may explain the data: one where dimers form and bind Notch receptors with heterodimers dominating the signaling, which we term the dimer scenario, and another one where monomers bind and activate Notch receptors directly, which we term the monomer scenario. In the dimer scenario, large-amplitude $K(t)$ oscillations are mainly driven by heterodimer $\kappa_E e(t)$ oscillations. The homodimer contributions $\kappa_F f(t)$ and $\kappa_G g(t)$ oscillate with a much smaller amplitude since κ_F and κ_G are an order of magnitude smaller than κ_E. Thus, this asserts a role of DeltaD as a binding partner in the heterodimer that is the main activator of Notch receptors. In the monomer scenario, $\kappa_D d(t)$ is relatively constant and $\kappa_C c(t)$ contributes the oscillatory component of $K(t)$. This suggests that the role of DeltaD in this case is to provide a signaling baseline that shifts $K(t)$ oscillations to larger absolute levels. In this interpretation, levels of $\kappa_C c(t)$ alone are not enough to synchronize the system, causing the DeltaD mutant phenotype. In these distinct ways, the two scenarios satisfy a common requirement of producing large-amplitude oscillations of the signal-carrying ligand binding activity $K(t)$. These oscillations of the ligand binding activity drive the signal $s(t)$ in Eq. (1) to periodically pass the threshold given by the dimensionless concentration scale σ and synchronize the oscillators.

The distinct roles of DeltaD in each scenario prompt us to look for possible differences in DeltaD dynamics. In the dimer scenario, DeltaD is present both as a monomer and as component of dimers. We find that the total DeltaD dimensionless concentration $d_T(t) = d(t) + e(t) + 2g(t)$ displays pronounced oscillations [Fig. 7(b)]. In contrast, in the monomer scenario $d_T(t) = d(t)$ displays small amplitude oscillations. We quantify the relative amplitude as the peak to trough difference over the average value of the oscillation, which results in a 71% and 7% relative amplitude in the dimer and monomer scenarios, respectively.

Upon binding of a ligand to a Notch receptor, the receptor is cleaved and NICD is released in the signal receiving cell, while the remaining part of the receptor forms a complex with the ligand that is internalized into the signal sending cell. The model so far does not describe the dynamics of this complex because it does not play any role in signaling [62,75]. However, to account for the total DeltaD present in a given cell, it may be important to include the ligand present in the internalized complex. We do this by considering that the ligand is recycled after internalization [62] or that the complex degrades faster than the ligand [86] or at the same rate [84] (Appendix E). Results in Fig. 7(b) correspond to instantaneous degradation of the complex. Although total DeltaD oscillations display lower relative amplitude in all other cases, the distinct behavior of dimer and monomer scenarios is preserved [Fig. S6 and Table S1] [68].

Given the distinct role of DeltaD in each scenario, we sought to identify perturbations that could supplant DeltaD in one role but not the other and might be experimentally realized. One such possibility is to supply a surrogate baseline for the DeltaC monomer in the absence of DeltaD, but that would not work as the strongly binding partner for DeltaC required in the dimer scenario. To test this idea, we included in the model an additional synthesis term for $s(t)$,

$$\dot{s}_i = -\delta_S s_i + K n_i + \beta_S, \tag{14}$$

where β_S represents an exogenous, unregulated expression of the NICD. Synchronization maps reveal that there is a range of values of β_S that rescue the DeltaD mutant phenotype in the monomer scenario, red dot and dashed line in Fig. 8(a). In

contrast, this NICD overexpression assay does not rescue the mutant in the dimer scenario [Fig. 8(b)]. The order parameter along the β_S direction shows a range of consistently high values above threshold R_T for the monomer case, while for dimers we observe large fluctuations that stay below threshold [Fig. 8 (bottom)]. Another possible perturbation is expressing exogenous unregulated DeltaC ligands, which results in a similar prediction distinguishing the two scenarios [Fig. S7] [68]. Taken together, these results provide a set of possible experiments that could test the two scenarios.

X. DISCUSSION

In this work we address the role of DeltaD in the synchronization of the zebrafish segmentation clock. Motivated by available experimental data, we first consider a model where ligands have to dimerize to bind the receptor and deliver a signal to a neighboring cell [34]. This seems a plausible idea since it provides a clear role for DeltaD as partner of DeltaC, making it necessary for synchronization. We show that this hypothesis is compatible with data from mutants, both steady-state and transient desynchronization phenotypes. While the key component in this hypothesis is the heterodimer, we find that homodimers are also required to explain the differences in transient desynchronization of ligand mutants. Since evidence for ligand dimers is limited, and mostly restricted to extraembryonic assays, we then test an alternative hypothesis where monomers directly bind and activate the Notch receptor. We show that this model is also consistent with data, providing a role for DeltaD as a baseline signal. These two different coupling hypotheses endow DeltaD with distinct roles. Following this, we discuss experiments that could distinguish between the two coupling hypotheses.

The key distinction of the two scenarios is the formation of dimers that have a prominent role in binding the Notch receptors. Dimerization of ligands has been demonstrated *in vitro* using antibodies for DeltaC and DeltaD [34]. More recently, ligand dimerization has also been reported in cell culture assays [74,87]. This work suggested that monomers bind Notch and drive *trans*-activation in neighbors while dimers mediate *cis*-inhibition. While *in vivo* colocalization has been suggested in zebrafish PSM using standard fluorescence immunohistochemistry [34], this technique has limited spatial resolution and it would be important to determine whether these dimers form as molecular species in the PSM as well, for example, using a FRET assay to test ligand proximity [88] or the N&B proximity assay to test oligomerization state [89]. Direct observation of *in vivo* molecular dimerization would be a strong indication for a role of dimers, in favor of the dimer scenario.

Additionally, the two scenarios predict different dynamics for total DeltaD concentrations. In the dimer scenario, DeltaD is expected to display pronounced oscillations. In contrast, only a weak undulation is expected in the monomer scenario. These results hold for different hypotheses regarding the fate of the internalized ligand and receptor in the signal sending cell. Thus, a possible test between the two scenarios is to image a transgenic DeltaD protein reporter *in vivo*, or use antibodies, to quantify the relative amplitude of DeltaD reporter fluctuations. Previous work using a DeltaD tagged with *venus*-YFP did not report such oscillations [35]. While this seems to favor the monomer scenario over the dimer scenario, additional experiments will be required to settle the question.

Motivated by the distinct roles of DeltaD in both coupling hypotheses, we showed that it should be possible to provide surrogates to rescue the DeltaD mutant. One possibility is to express the NICD independently of regulatory interactions. This could be done by synthetic biology approaches that introduce engineered forms of the Notch receptor [90–92]. A constant level of NICD signaling or unregulated DeltaC overexpression would provide a baseline for endogenous DeltaC in the monomer scenario but would fail to provide the binding partner for DeltaC in the dimer binding case. A similar strategy would be to express exogenous DeltaC at constant levels, independent of the Her-inhibited DeltaC. In the monomer binding case, this additional supply of constantly expressed DeltaC would provide a baseline, whereas in the dimer binding case it would not be doing the job of the missing DeltaD, since DeltaC homodimerization is thought to be much weaker [34]. In the embryo, this could be approached by *deltaC* mRNA injection, providing a pool of mRNA for translation. Previous experiments using this strategy showed that injecting deltaC mRNA into either *deltaC* or *deltaD* heterzygotes does not improve recovery in a DAPT pulse assay, whereas injecting deltaD mRNA into the *deltaD* heterzygote does [64]. While these experiments revealed distinct roles for DeltaC and DeltaD ligands, the failure to rescue by deltaC mRNA is not conclusive because according to the theory rescue is nonmonotonic with mRNA concentration. A thorough test will require titrating the mRNA concentration to scan the region of possible rescue in the monomer scenario. A limitation of this approach may be the mRNA stability, which would introduce a decreasing synthesis rate for the protein. An alternative to circumvent this problem would be to generate a transgenic line with a constitutively expressed DeltaC or introducing DeltaC copies with a DeltaD promoter. The reciprocal experiment, in which a DeltaC mutant is supplemented with a DeltaD transgene, should not rescue the desynchronization phenotype.

In the theory, a single oscillatory ligand like DeltaC can synchronize oscillations in the absence of DeltaD, if its synthesis rate is large enough. However, in the zebrafish embryo the DeltaC ligand alone has a desynchronization phenotype [12]. The 30-min period constraint imposed by the clock timing [93] may require fast biochemical kinetics of the oscillating DeltaC ligand, limiting its amplitude and consequently leading to the requirement for a two ligand scheme. Such a scheme may also confer additional properties, such as flexibility [94] to tune a coupling profile across the unsegmented tissue [95], similarly to the frequency [96] and mobility [65] profiles. Finally, these ligands have other roles in other biological contexts, likely setting additional constraints on the biochemistry and kinetics outside of those required for segmentation clock synchronization. For example, coexpression of DeltaC and DeltaD ligands is found in developing retinal cells [34]; DeltaA and DeltaD are coexpressed in neural plate [86]; and DeltaA, DeltaC, and DeltaD are concomitantly found in neuronal progenitors during spinal cord development [97]. Indeed, combinatorial coexpression of multiple components of the Notch pathway is ubiquitous [98].

Notch ligands have a differential role in other contexts as well [99–102]. In cancer cells, a differential synthesis rate for Notch ligands Delta and Jagged was proposed to drive the formation of cell clusters that enhance metastasis [100]. In a more generic context, the roles of interacting cells as signal senders or receivers is also controlled by the amount of available Delta and Jagged, which results in the Notch-Delta-Jagged network playing a decisive role in lateral inhibition-based pattern formation [101]. Another proposal is that ligand binding efficiency of two generic ligands and competition for the same Notch binding may result in new signaling states, underlying signaling robustness and versatility [102]. It would be interesting to consider these scenarios in the context of the segmentation clock in future work.

A recent study generated a library of engineered cell lines to characterize the modes of ligand receptor interaction for four different ligands and two receptors found in mammalian cells [103]. The study revealed a range of *cis*- and *trans*-inhibition and -activation for different concentrations. It has also been shown that Notch *cis*-inhibition or -activation plays a key role in cell-fate decisions and patterning [52,74,84,104], and a role for *cis*-inhibition has been reported in the mouse segmentation clock [78]. Although there is currently no evidence for this in the zebrafish segmentation clock, the evidence from mouse together with the orthology of mouse and zebrafish Delta ligands, prompted us to consider the effects of *cis*-inhibition in the context of the monomer scenario. We showed that *cis* interactions endow the ligand DeltaD with a distinct role in synchronization by modulating its availability. However, this could not account for the differences in desynchronization phenotypes observed in the zebrafish. In this work, we considered monomer mediated *cis*-inhibition. We expect that dimer mediated *cis*-inhibition [74] could have a similar effect on synchronization, since dimerization introduces an additional intermediate step in the interaction. Future research could consider this possibility, and additional *cis* interactions through heterodimers [87], in the context of synchronization.

Notch signaling is well known for its diverse roles in a wide range of developmental processes and in disease [5,9,105]. For example, in coordinating antiphase oscillations during neurogenesis [106,107], oscillations in fate decision of pancreatic progenitors [108], patterning of the retina [109,110], the neurogenic wavefront in the chick retina [111], blood cell fate decisions [112], tissue regeneration [113], and adult neurogenesis [114]. This remarkable versatility of Notch signaling in different contexts remains an interesting open question. Understanding how cells use ligand multiplicity to communicate in different contexts will be relevant to medical applications such as diagnostics and therapeutics, as well as to harness this versatility for applications in gastruloid and organoid biology and tissue engineering [19,115–118].

ACKNOWLEDGMENTS

We thank Bo-Kai Liao for fruitful discussions on the role of DeltaD, Melina Magalnik for illuminating conversations on experimental tests of the theory, and Margulis for entertaining contributions during discussions across timezones. This work was supported by ANPCyT Grants No. PICT 2017 3753 and No. PICT 2019 0445 awarded to L.G.M. and FOCEM-Mercosur (COF 03/11) to IBioBA. M.W. was supported by a CONICET fellowship and L.G.M. is a researcher of CONICET. K.U. was supported by the JSPS KAKENHI Grants No. 23K27213 and No. 24H00863. A.C.O. was supported by SNSF division III project 31003A_176037. L.G.M. thanks JSPS Long Term Invitational Fellowship L23529 and the Uriu Lab at Tokyo Tech for hospitality.

APPENDIX A: REACTION KINETICS AND MODEL FORMULATION

1. Regulatory function

This work focuses on the roles of different components of the Notch signaling network, so we take a parsimonious approach to describe the core oscillator. We consider a single Her protein that inhibits its own production with a time delay accounting for synthesis time. The single variable $H(t)$ represents the concentration of this protein at time t. Besides self-inhibition, the synthesis rate of Her protein is positively regulated by Notch signaling components. The NICD is released inside the cell upon binding of ligands from neighboring cells to the Notch receptor. We denote the concentration of this signaling component by $S(t)$.

Here we derive a function to describe the regulatory effects of H and S on the synthesis rate of H. We will first consider the dynamics and steady state of the promoter and the binding factors. The promoter architecture of *her* genes may be complex, including about 12 binding sites for the Her proteins [25]. Besides, it is thought that Her proteins bind as dimers to their own promoters [25]. It has been shown that multiple binding sites effectively increase the nonlinearity of regulatory functions [119–121]. Similarly, dimerization can be effectively described in an adiabatic approximation by a Hill exponent of 2 [25]. Thus, here we assume that there is only one binding site for Her proteins for simplicity, and then include the effects of multiplicity in an effective Hill exponent [119]. We further assume that NICD binds as a single molecule to the activating complex at the Her promoter.

With these assumptions, the promoter can be in any of four states, depending on whether none, one, or both of the binding sites are occupied. We represent the promoter state as $P_{\mu\nu}$, where μ is the state of the Her binding site and ν is the state of the NICD binding site, with $\mu, \nu = 0$ indicating an empty site and $\mu, \nu = 1$ an occupied site. The different promoter states are connected in the scheme of binding reactions

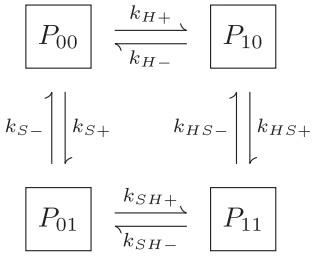

where the $+$ and $-$ signs label binding and unbinding rates respectively. The values of $k_{HS\pm}$ and $k_{SH\pm}$ depend on how the two regulatory components interact. For instance, setting them both to zero, $k_{HS+} = k_{SH+} = 0$ describes exclusive competi-

tive binding, where the doubly bound promoter state is not accessible [122]. Alternatively, assuming the binding rates to be independent of the promoter state for both components, $k_{SH\pm} = k_{H\pm}$ and $k_{HS\pm} = k_{S\pm}$, describes a situation with no interaction at the binding sites of regulatory components, which we term dual binding model. Further choices describe models for different ligand interactions. Motivated by the multiple binding sites accessible to Her transcription factors, here we focus on the dual binding model. The reactions involved are

$$P_{00} + H \underset{k_{H-}}{\overset{k_{H+}}{\rightleftharpoons}} P_{10}, \quad P_{10} + S \underset{k_{S-}}{\overset{k_{S+}}{\rightleftharpoons}} P_{11}, \tag{A1}$$

$$P_{00} + S \underset{k_{S-}}{\overset{k_{S+}}{\rightleftharpoons}} P_{01}, \quad P_{01} + H \underset{k_{H-}}{\overset{k_{H+}}{\rightleftharpoons}} P_{11}. \tag{A2}$$

From these reactions we can write the dynamics for the four states of the promoter,

$$\dot{P}_{00} = k_{H-}P_{10} + k_{S-}P_{01} - k_{H+}HP_{00} - k_{S+}SP_{00}, \tag{A3}$$

$$\dot{P}_{10} = k_{H+}HP_{00} + k_{S-}P_{11} - k_{H-}P_{10} - k_{S+}SP_{10}, \tag{A4}$$

$$\dot{P}_{01} = k_{S+}SP_{00} + k_{H-}P_{11} - k_{S-}P_{01} - k_{H+}HP_{01}, \tag{A5}$$

$$\dot{P}_{11} = k_{H+}HP_{01} + k_{S+}SP_{10} - k_{H-}P_{11} - k_{S-}P_{11}, \tag{A6}$$

together with the conservation law

$$P_{00} + P_{10} + P_{01} + P_{11} = P_T. \tag{A7}$$

We assume that promoter binding and unbinding reactions are much faster than the dynamics of H and S. With this assumption, the promoter state is in equilibrium for given concentrations of H and S and we set $\dot{P}_{\mu\nu} = 0\ \forall \mu, \nu$. We can solve the resulting algebraic equations to obtain the quasi-steady-state promoter occupancy $P_{\mu\nu}(H, S)$,

$$P_{00}(H,S) = \frac{k_{H-}k_{S-}P_T}{(k_{H-}+k_{H+}H)(k_{S-}+k_{S+}S)}, \tag{A8}$$

$$P_{10}(H,S) = \frac{k_{S-}k_{H+}P_T H}{(k_{H-}+k_{H+}H)(k_{S-}+k_{S+}S)}, \tag{A9}$$

$$P_{01}(H,S) = \frac{k_{H-}k_{S+}P_T S}{(k_{H-}+k_{H+}H)(k_{S-}+k_{S+}S)}, \tag{A10}$$

$$P_{11}(H,S) = \frac{k_{H+}k_{S+}P_T HS}{(k_{H-}+k_{H+}H)(k_{S-}+k_{S+}S)}. \tag{A11}$$

Next, we consider how promoter occupancy determines transcription rates. We introduce the regulatory function $f(H, S)$ that modulates the synthesis rate of H,

$$f(H,S) = \sum_{\mu,\nu=0,1} a_{\mu\nu}P_{\mu\nu}(H,S), \tag{A12}$$

where each promoter state $P_{\mu\nu}$ has an associated transcription rate $a_{\mu\nu}$. Here assume that binding of Her to the promoter fully represses synthesis independently of the binding of NICD, $a_{10} = a_{11} = 0$. We set a basal transcription rate $a_{00} = b$ and an activated state to a higher rate $a_{01} = a > b$, resulting in

$$f(H,S) = P_T\frac{k_{H-}(bk_{S-} + ak_{S+}S)}{(k_{H-}+k_{H+}H)(k_{S-}+k_{S+}S)}. \tag{A13}$$

Introducing concentration scales

$$H_0 \equiv \frac{k_{H-}}{k_{H+}} \quad \text{and} \quad S_0 \equiv \frac{k_{S-}}{k_{S+}}, \tag{A14}$$

we arrive at

$$f(H,S) = \frac{b_H}{1+\frac{H}{H_0}}\frac{1+\frac{a_H}{b_H}\frac{S}{S_0}}{1+\frac{S}{S_0}}, \tag{A15}$$

where we defined $a_H \equiv P_T a$ and $b_H \equiv P_T b$.

This expression provides the structure of the regulatory function. As we described above, Her proteins form dimers and these dimers bind to multiple binding sites on the promoter. Similarly, the NICD binds DNA through a complex that may also introduce additional nonlinearities. These effects can be encompassed in effective Hill exponents h_H and h_S,

$$f(H,S) = b_H\frac{1}{1+\left(\frac{H}{H_0}\right)^{h_H}}\frac{1+\frac{a_H}{b_H}\left(\frac{S}{S_0}\right)^{h_S}}{1+\left(\frac{S}{S_0}\right)^{h_S}}. \tag{A16}$$

The regulatory function separates into factors,

$$f_-(H) = \frac{1}{1+\left(\frac{H}{H_0}\right)^{h_H}} \quad \text{and} \quad f_+(S) = \frac{1+\frac{a_H}{b_H}\left(\frac{S}{S_0}\right)^{h_S}}{1+\left(\frac{S}{S_0}\right)^{h_S}}, \tag{A17}$$

such that

$$f(H,S) = b_H f_-(H) f_+(S), \tag{A18}$$

reflecting the independent binding assumption, where binding to one site is independent of the state of the other.

Next, to complete the formulation of the model, we describe the different reactions involved, from synthesis to degradation, ligand dimerization, and Notch binding by different components.

2. Synthesis

Her synthesis proceeds at a basal rate b_H, modulated by the regulatory function Eq. (A16),

$$\dot{H}_i(t) = b_H\frac{1}{1+\left(\frac{H_i(t-\tau_i)}{H_0}\right)^{h_H}}\frac{1+\frac{a_H}{b_H}\left(\frac{S_i(t-\tau_i)}{S_0}\right)^{h_S}}{1+\left(\frac{S_i(t-\tau_i)}{S_0}\right)^{h_S}} + \cdots, \tag{A19}$$

where $i = 1, \ldots, N_c$ is the cell label and τ_i is an explicit synthesis delay accounting for the multiple steps in the negative feedback of H [123,124]. Since a Her molecule takes a time τ_i to be synthesized in cell i, the synthesis rate at time t depends on Her and NICD concentrations at a previous time $t - \tau_i$, when synthesis was starting. This delay is different for each cell, introducing a variability in the period of the cell population as described below.

To describe DeltaC synthesis inhibition by Her, we follow a similar strategy as above. Considering the reaction kinetics for the binding of Her to the DeltaC promoter,

$$\dot{C}_i(t) = b_C\frac{1}{1+\left(\frac{H_i(t-\tau_C)}{H_{0C}}\right)^{h_C}} + \cdots, \tag{A20}$$

where b_C is the basal rate, τ_C is the DeltaC synthesis delay, H_{0C} is the threshold for Her mediated inhibition of DeltaC synthesis and h_C is an effective Hill exponent describing nonlinear effects in the inhibition. Finally, we set constant synthesis rates for DeltaD and Notch, since they are not regulated by other components from the oscillator or the coupling

network, resulting in constant terms

$$\dot{D}_i(t) = b_D + \cdots \quad \text{and} \quad \dot{N}_i(t) = b_N + \cdots . \tag{A21}$$

3. Degradation

We assume decay of all components according to the reactions

$$X \xrightarrow{d_X} \varnothing, \tag{A22}$$

resulting in a linear decay term

$$\dot{X}_i(t) = -d_X X_i(t) + \cdots \tag{A23}$$

for all variables $X = H, C, D, E, F, G, N, S$, where d_X is the decay rate for the variable X.

4. Ligands dimerization

Notch ligands DeltaC and DeltaD can form an heterodimer and both homodimers, described in the reactions

$$\mathrm{C}_i + \mathrm{D}_i \underset{\mathrm{k}^-_{\mathrm{CD}}}{\overset{\mathrm{k}^+_{\mathrm{CD}}}{\rightleftharpoons}} \mathrm{C:D_i}, \tag{A24}$$

$$2\mathrm{C}_i \underset{\mathrm{k}^-_{\mathrm{CC}}}{\overset{\mathrm{k}^+_{\mathrm{CC}}}{\rightleftharpoons}} \mathrm{C:C_i}, \tag{A25}$$

$$2\mathrm{D}_i \underset{\mathrm{k}^-_{\mathrm{DD}}}{\overset{\mathrm{k}^+_{\mathrm{DD}}}{\rightleftharpoons}} \mathrm{D:D_i}. \tag{A26}$$

We introduce the notation for dimers concentrations, [DeltaC:DeltaD] $\equiv E$, [DeltaC:DeltaC] $\equiv F$, [DeltaD:DeltaD] $\equiv G$, and relabel the corresponding rates as $k^{\pm}_E \equiv k^{\pm}_{CD}$, $k^{\pm}_F \equiv k^{\pm}_{CC}$, and $k^{\pm}_G \equiv k^{\pm}_{DD}$. Each reaction contributes terms to the components involved. For example, Eq. (A25) will contribute terms to the equations for the DeltaC monomer and the DeltaC:DeltaC homodimer,

$$\dot{C}_i(t) = -2k^+_F C_i^2 + 2k^-_F F_i + \cdots , \tag{A27}$$

$$\dot{F}_i(t) = +k^+_F C_i^2 - k^-_F F_i + \cdots . \tag{A28}$$

5. Notch binding

Ligands from a neighboring cell, in the form of monomers or dimers, may bind to a Notch receptor. Once Notch is bound by a ligand, its intracellular domain is released into the cell and the complex formed by the remaining extracellular domain and the bound ligand is internalized into the other cell. Here we assume that the ligand is degraded after the interaction with a receptor. Since the receptor is cleaved in the process, we describe this as an irreversible reaction,

$$\mathrm{X}_i + \mathrm{N}_j \xrightarrow{\mathrm{k_{NX}}} \mathrm{S}_j, \quad \mathrm{X = C,D,E,F,G}, \tag{A29}$$

where k_{NX} is the binding rate between Notch and a ligand X, and i, j label the interacting cells.

6. Average neighbor coupling

These Notch binding reactions give rise to the coupling terms in the dynamics of X,

$$\dot{X}_i(t) = -\sum_{j\in\mathcal{V}_i} k_{NX} X_i N_j r_{ij} + \cdots , \tag{A30}$$

where the sum is over neighbors $\mathcal{V}_i$ of cell i. The contribution from each neighbor j is weighted by the fraction r_{ij} of the total surface of cell i in contact with cell j,

$$r_{ij} = \frac{A_{ij}}{A_T}, \tag{A31}$$

where A_{ij} is the contact area between the two neighbors and A_T is the total area of a cell, assumed to be the same for all cells. Assuming that the total cell i area is shared equally with all $|\mathcal{V}_i|$ neighbors, $A_{ij} = A_T/|\mathcal{V}_i|$, and

$$r_{ij} = \frac{1}{|\mathcal{V}_i|}. \tag{A32}$$

With this assumption, cell i is coupled to the average of Notch concentrations in neighboring cells,

$$\dot{X}_i(t) = -k_{NX} X_i \frac{1}{|\mathcal{V}_i|} \sum_{j\in\mathcal{V}_i} N_j + \cdots . \tag{A33}$$

Similar average couplings arise in the equations for N and S,

$$\dot{N}_i(t) = -k_{NX} N_i \frac{1}{|\mathcal{V}_i|} \sum_{j\in\mathcal{V}_i} X_j + \cdots , \tag{A34}$$

$$\dot{S}_i(t) = +k_{NX} N_i \frac{1}{|\mathcal{V}_i|} \sum_{j\in\mathcal{V}_i} X_j + \cdots . \tag{A35}$$

7. Mean field

In this work we focus on the tailbud, a posterior region of the segmentation clock characterized by synchronized oscillations in a population of very mobile cells [65]. This cell mobility causes a continuous neighbor exchange, and it has been shown that the resulting dynamics can be effectively described as an all-to-all coupling or mean field [41]. Thus, we write the average terms in Eqs. (A33)–(A35) for the ligands and the Notch receptor as mean-field variables,

$$\bar{X} = \frac{1}{N_c} \sum_{i=1}^{N_c} X_i, \quad X = C, D, E, F, G, N. \tag{A36}$$

With these definitions, we can write the gain and loss terms that reactions in Eq. (A29) contribute to different components. For example, the heterodimer E participates in the contributions as follows:

$$\dot{S}_i(t) = +k_{NE} \bar{E} N_i + \cdots , \tag{A37}$$

$$\dot{E}_i(t) = -k_{NE} E_i \bar{N} + \cdots , \tag{A38}$$

$$\dot{N}_i(t) = -k_{NE} \bar{E} N_i + \cdots . \tag{A39}$$

8. Full model

Putting all contributions together, we have eight coupled delayed differential equations for each cell i,

$$\dot{H}_i = -d_H H_i + b_H \frac{1}{1 + \left(\frac{H_i(t-\tau_i)}{H_0}\right)^{h_H}} \frac{1 + \frac{a_H}{b_H}\left(\frac{S_i(t-\tau_i)}{S_0}\right)^{h_S}}{1 + \left(\frac{S_i(t-\tau_i)}{S_0}\right)^{h_S}}, \tag{A40}$$

$$\dot{C}_i = -d_C C_i + b_C \frac{1}{1 + \left(\frac{H_i(t-\tau_C)}{H_{0C}}\right)^{h_C}} - k^+_E C_i D_i + k^-_E E_i - 2k^+_F C_i^2 + 2k^-_F F_i - k_{CN} C_i \bar{N}, \tag{A41}$$

$$\dot{D}_i = -d_D D_i + b_D + k_E^- E_i - k_E^+ C_i D_i - 2k_G^+ D_i^2 + 2k_G^- G_i - k_{DN} D_i \bar{N}, \tag{A42}$$

$$\dot{E}_i = -d_E E_i - k_E^- E_i + k_E^+ C_i D_i - k_{EN} E_i \bar{N}, \tag{A43}$$

$$\dot{F}_i = -d_F F_i - k_F^- F_i + k_F^+ C_i^2 - k_{FN} F_i \bar{N}, \tag{A44}$$

$$\dot{G}_i = -d_G G_i - k_G^- G_i + k_G^+ D_i^2 - k_{GN} G_i \bar{N}, \tag{A45}$$

$$\dot{N}_i = -d_N N_i + b_N - k_{CN} \bar{C} N_i - k_{DN} \bar{D} N_i - k_{EN} \bar{E} N_i - k_{FN} \bar{F} N_i - k_{GN} \bar{G} N_i, \tag{A46}$$

$$\dot{S}_i = -d_S S_i + k_{CN} \bar{C} N_i + k_{DN} \bar{D} N_i + k_{EN} \bar{E} N_i + k_{FN} \bar{F} N_i + k_{GN} \bar{G} N_i, \tag{A47}$$

where we omit the time dependence for notational simplicity except in delayed contributions. This full model is a superset of all the special cases considered in the main text, including all possible dimers and Notch binding species. The scenarios considered in the main text can be obtained by an adequate choice of parameters. For instance, choosing the binding rates $k_{CN} = k_{DN} = 0$ gives us the dimer scenario of the main text, while choosing all dimerization constants $k_X^{\pm} = 0$ and the corresponding Notch coupling constants $k_{NX} = 0$ for $X = E, F, G$ results in the monomer scenario.

9. Period variability

The autonomous period of the core oscillator i depends primarily on the value of the synthesis delay τ_i in the negative feedback, and the half-life of the protein d_H^{-1}, with second-order corrections depending mainly on the synthesis rate b_H [22]. To introduce variability in the autonomous periods, we sample the delays τ_i of individual oscillators from a normal distribution, with mean τ_H and variance σ_τ.

10. DAPT assay

Notch signaling can be blocked by the drug DAPT which inhibits the proteolytic cleavage of the receptor and the consequent release of the NICD [13,14]. Above a saturating concentration $[\text{DAPT}]_{\text{sat}} \approx 50\ \mu\text{M}$, no information is transmitted via the Notch pathway [38]. We can simulate an assay in which a variable dose of DAPT is delivered to the embryo by including a factor in Eq. (2),

$$\dot{s}_i = -\delta_S s_i + n_i K\left(1 - \frac{[\text{DAPT}]}{[\text{DAPT}]_{\text{sat}}}\right), \tag{A48}$$

where [DAPT] is the applied concentration of DAPT. In desynchronziation assays, we set $[\text{DAPT}] = [\text{DAPT}]_{\text{sat}}$, which is equivalent to setting $K = 0$ in Eq. (2).

APPENDIX B: DIMENSIONLESS FORMULATION

Next, we introduce the dimensionless formulation of the model that we use in the main text, which provides a description that is independent of timescales and concentration scales. Equations (A40)–(A47) have units of concentration over time. We choose the concentration scale H_0 and the timescale d_H^{-1}, and render the equations dimensionless multiplying all by the same factor $(d_H H_0)^{-1}$. Introducing dimensionless variables

$$x_i \equiv \frac{X_i}{H_0}, \quad X = H, C, D, E, F, G, N, S, \tag{B1}$$

and dimensionless time

$$\tilde{t} \equiv t d_H, \tag{B2}$$

the time derivatives transform as

$$\frac{\dot{X}}{d_H H_0} = \frac{dx}{d\tilde{t}} \equiv x', \tag{B3}$$

where we defined the prime notation for the derivative with respect to $\tilde{t}$. The resulting dimensionless formulation is

$$h_i' = -h_i + \beta_h \frac{1}{\left[1 + h_i^{\eta_H}(\tilde{t} - \tilde{\tau}_i)\right]} \frac{1 + \alpha(\sigma s_i(\tilde{t} - \tilde{\tau}_i))^{\eta_S}}{\left[1 + (\sigma s_i(\tilde{t} - \tilde{\tau}_i))^{\eta_S}\right]}, \tag{B4}$$

$$c_i' = -\delta_c c_i + \beta_c \frac{1}{1 + (\gamma h_i(\tilde{t} - \tilde{\tau}_C))^{\eta_C}} + \lambda_E^- e_i - \lambda_E^+ c_i d_i + \lambda_F^- f_i - \lambda_F^+ c_i^2 - \kappa_C c_i \bar{n}, \tag{B5}$$

$$d_i' = -\delta_d d_i + \beta_d + \lambda_E^- e_i - \lambda_E^+ c_i d_i + \lambda_G^- g_i - \lambda_G^+ d_i^2 - \kappa_D d_i \bar{n}, \tag{B6}$$

$$e_i' = -\delta_e e_i - \lambda_E^- e_i + \lambda_E^+ c_i d_i - \kappa_E e_i \bar{n}, \tag{B7}$$

$$f_i' = -\delta_f f_i - \lambda_F^- f_i + \lambda_F^+ c_i^2 - \kappa_F f_i \bar{n}, \tag{B8}$$

$$g_i' = -\delta_G g_i - \lambda_G^- g_i + \lambda_G^+ d_i^2 - \kappa_G g_i \bar{n}, \tag{B9}$$

$$n_i' = -\delta_n n_i + \beta_n - n_i \sum_{c,d,e,f,g} \kappa_X \bar{x}, \tag{B10}$$

$$s_i' = -\delta_s s_i + n_i \sum_{x=c,d,e,f,g} \kappa_X \bar{x}, \tag{B11}$$

with dimensionless parameters

$$\delta_X \equiv \frac{d_X}{d_H}, \quad \beta_X = \frac{b_X}{d_H H_0}, \quad \kappa_X = \frac{k_{XN} H_0}{d_H}, \quad \sigma = \frac{H_0}{S_0}, \quad \gamma \equiv \frac{H_0}{H_{0C}}, \quad \alpha = \frac{a_H}{b_H},$$

$$\lambda_E^+ \equiv \frac{H_0 k_E^+}{d_H}, \quad \lambda_E^- \equiv \frac{k_E^-}{d_H}, \quad \lambda_F^+ \equiv \frac{2H_0 k_F^+}{d_H}, \quad \lambda_F^- \equiv \frac{2k_F^-}{d_H}, \quad \lambda_G^+ \equiv \frac{2H_0 k_G^+}{d_H}, \quad \lambda_G^- \equiv \frac{2k_G^-}{d_H}.$$

and renaming $h_X \to \eta_X, X = H, S, C$. For notational simplicity and readability, in the main text we drop the tildes from dimensionless time variables $\tilde{t} \to t$ and $\tilde{\tau}_X \to \tau_X$. We also drop the prime notation and use a dot to denote dimensionless time derivatives.

APPENDIX C: PARAMETER VALUES

Next we parametrize the model to describe both wildtype and mutant conditions. Experimental observations of the zebrafish segmentation clock, together with theoretical considerations, set constraints on parameter values. To parametrize the core oscillator we follow [22], comparing the mRNA and protein model,

$$\dot{p}(t) = am(t-\tau_p) - bp(t), \tag{C1}$$

$$\dot{m}(t) = \frac{k}{1+\left(\frac{p(t-\tau_m)}{p_0}\right)^n} - cm(t), \tag{C2}$$

to the protein only oscillator from Eq. (B4),

$$\dot{H}(t) = -d_H H(t) + \frac{b_H}{1+\left(\frac{H(t-\tau_H)}{H_0}\right)^{\eta_H}}. \tag{C3}$$

Parameter values estimated for the mRNA and protein oscillator are [22]: $a = 4.5$ proteins per mRNA molecule, $c = 0.23$ molecules per minute, $b = 0.286$ molecules per minute estimated from experiments [55], $k = 33$ mRNA molecules per diploid cell per minute, and $p_0 = 40$ molecules. Synthesis delays in the model were later estimated from experiments [125], showing that her1 and her7 have very similar transcription times $\tau_{m1} \approx 10$ min and $\tau_{m7} \approx 9$ min, dominating over the protein translation times $\tau_{p1} \approx 2.8$ min and $\tau_{p7} \approx 1.7$ min.

Introducing a quasi-steady-state approximation for the mRNA, $\dot{m} \approx 0$, we obtain

$$m(t) \approx \frac{k}{c}\frac{1}{1+\left(\frac{p(t-\tau_m)}{p_0}\right)^n}, \tag{C4}$$

and replacing $m(t-\tau_p)$ into (C1),

$$\dot{p}(t) = -bp(t) + \frac{ak}{c}\frac{1}{1+\left(\frac{p(t-\tau_m-\tau_p)}{p_0}\right)^n}. \tag{C5}$$

Comparing Eqs. (C3) and (C5) we see that to obtain similar dynamics we should set $d_H \approx b$, $b_H \approx ak/c$, $\tau_H \approx \tau_m + \tau_p$, $\eta_H \approx n$ and $H_0 \approx p_0$. Since this comparison relies on the quasi-steady-state approximation, a strict assignment of these values may produce differences in amplitude and period. In addition, the synthesis delay τ_H could be estimated differently from comparing the estimated period for both models,

$$T_{\text{Lewis}} \approx 2(\tau_p + \tau_m + 1/b + 1/c), \tag{C6}$$

$$T_H \approx 2(\tau_H + 1/d_H). \tag{C7}$$

For these periods to match, we would require $\tau_H \approx \tau_m + \tau_p + 1/c$.

For the protein only model, parameter values from Ref. [22] imply a Her protein degradation rate $d_H = 0.286\ \text{min}^{-1}$, setting the timescale, and $H_0 = p_0 = 40$ molecules, corresponding to a concentration scale $[H_0] \approx 0.3$ nM for tailbud cells of 7.6 μm in diameter [65]. To obtain oscillations of similar amplitude to Ref. [22], we set $\beta_H = 28$ in the dimensionless model, corresponding to $b_H \approx 320$ proteins per minute. We set the dimensionless delay to $\tau_h = 4.2$, corresponding to a synthesis delay within a range of values obtained from averaging Her1 and Her7 data, $\tau_H = 14.7$. Hill exponents have an effective value that encompasses the effect of multiple macromolecular interactions in the regulation, such as dimerization [25], binding of complexes and multiple binding sites at the promoter [119,120]. We expect exponent values to be larger than 2, so we set the conservative estimate $\eta = 2.5$. We will use these values for the core oscillator and determine the rest of parameters from further estimations and explorations.

The rest of the parameters concern signaling components, such as the ligands DeltaC and DeltaD, their dimerization, binding to Notch receptors and signal production and action on the oscillator. We set some of these parameters below and explore the effects of varying others.

Next we consider signal reception parameters in Eq. (B4). The dimensionless threshold for signal-driven synthesis activation σ controls how much signal is necessary to affect the core oscillator. We chose a value $\sigma = 0.1$, which corresponds to a weaker action than the inhibitor. For the signal to activate Her protein synthesis above basal levels we require a coupling strength $\alpha > 1$. Through exploration, we settled for a value $\alpha = 10$, which increases Her collective oscillation amplitude by a factor of ∼2. The corresponding Hill exponent η_S was set equal to η_H for simplicity.

In the regulation of DeltaC synthesis by Her protein Eq. (B5), we set the dimensionless threshold for synthesis repression $\gamma = 1$, assuming for simplicity that the same concentration of Her protein is required to inhibit both Her and DeltaC synthesis. Experimental observations in zebrafish showed that impairing Notch signaling results in longer collective period [38]. For reduced coupling to lengthen the period, effective coupling delays should be slightly below the period value [37,126]. With this motivation we set the synthesis delay of DeltaC to $\tau_C = 1.7\tau_H$. The corresponding Hill exponent η_C was set equal to η_H for simplicity.

Given the lack of specific data for each component, we set all decay rates in the model to the same value $d_X = d_H$ with $X \in \{C, D, E, F, G, N, S\}$, for simplicity. So $\delta_X = 1$ for all X in the dimensionless model. Motivated by experimental observations, we set the values of dimerization and binding rates to Notch of the two homodimers about an order or magnitude lower than those of the heterodimer [34]. Scans of these parameters revealed that dimer association rates λ_X^+ have maximal effective values: Beyond some level, the size of the synchronization region in β_C vs β_D space stops changing significantly. Dimer dissociation rates λ_X^- were found to have small effects on the size and shape of the synchronization regions as long as they where within an order of magnitude of the corresponding λ_X^+, and were set to $\lambda_X^- = 0.1$.

The remaining parameters are the synthesis rates of coupling components and the binding rates of different components to Notch receptors. We vary synthesis rates β_C, β_D, and β_N to construct synchronization maps in terms of these. Additionally, we vary the values of κ_X to explore how these maps change.

We set wildtype parameters so that mutant conditions are consistent with experimental data. In the embryo, DeltaC and DeltaD mutants have mean ALDs of about 5.5 and 8, respectively. In the dimer scenario, we first simulate the DeltaC mutant condition, setting $\beta_C = 0$, to determine its ALD value. Since in the absence of DeltaC there is no oscillatory signal

delivered to neighboring cells, the ALD of this DeltaC mutant is primarily determined by the spread of the period distribution, and is not affected by parameters β_D and β_N. Next, we look for β_N and β_C values such that DeltaD mutant condition has a mean ALD about 2.5 segments larger than that of the DeltaC mutant. To simulate DeltaD mutant we set $\beta_D = 0$, set a β_N value, and plot ALD as a function of β_C, Figs. S5(a) and S5(c) [68]. We construct these curves for different values of β_N, and for each curve we select a wildtype β_C^{WT} value that satisfies the ALD constraint between the mutants, gray line in Fig. S5(a) and S5(c) [68]. We choose β_N^{WT} and β_C^{WT} to have similar values. Finally, we choose a wildtype value β_D^{WT} so that the corresponding Kuramoto order parameter is within the range of large values, reflecting a higher level of steady-state synchrony. With this choice, variations in β_D of about 30% do not impair wildtype synchrony levels. To place the Notch mutant condition in the synchronization map, we decrease β_N until we find the value that satisfies the experimental ALD of about 8, gray line in Fig. S5(b) and S5(d) [68].

For the monomer scenario, we first set β_D to be similar to the value of the dimer scenario, and chose a value for β_N within the range that allows for steady-state desynchronization of the DeltaD mutant. Then we determined the value of β_C to match the experimental ALDs. The existence of asymmetries between parameters for DeltaC and DeltaD synthesis and Notch binding are also consistent with experimental resynchronization assays, in which differences in ligand activities were reported [64].

APPENDIX D: *CIS*-INHIBITION

Cis interactions are binding events of a ligand to a receptor within the same cell. Notch *cis*-inhibition has been proposed to play a role in different contexts and model systems. We consider *cis* interactions between ligand monomers and Notch in the same cell i through the reaction

$$X_i + N_i \underset{k_X^-}{\overset{k_X^+}{\rightleftharpoons}} [X_i : N_i] \xrightarrow{d_{XN}} \varnothing, \tag{D1}$$

for $X = C, D$, where $k_X^{\pm}$ are association (+) and dissociation (−) rates for the *cis* complex $[X_i : N_i]$. We assume the complex decays linearly with a rate d_{XN}, effectively taking the ligand and Notch out of the system. The dynamics of the complex is given by

$$\frac{d}{dt}[X_i : N_i] = -d_{XN}[X_i : N_i] + k_X^+ X_i N_i - k_X^-[X_i : N_i], \tag{D2}$$

and complementary terms are added to Eqs. (A41), (A42), and (A46) for ligand X_i and receptor N_i in the form

$$\dot{X}_i = \ldots - k_X^+ X_i N_i + k_X^-[X_i : N_i], \tag{D3}$$

$$\dot{N}_i = \ldots - k_X^+ X_i N_i + k_X^-[X_i : N_i]. \tag{D4}$$

Assuming the dynamics of the complex is much slower than the oscillations, we use a quasi-steady-state approximation in Eq. (D2) and obtain

$$[X_i : N_i] = \frac{k_X^+}{k_X^- + d_{XN}} X_i N_i. \tag{D5}$$

We substitute this value into Eqs. (D3) and (D4),

$$\dot{X}_i = \ldots - k_{XN}^{\mathrm{cis}} X_i N_i, \tag{D6}$$

$$\dot{N}_i = \ldots - k_{XN}^{\mathrm{cis}} X_i N_i, \tag{D7}$$

where we introduced the effective *cis*-binding rate of ligand X to Notch

$$k_{XN}^{\mathrm{cis}} \equiv d_{XN} \frac{k_x^+}{k_x^- + d_{XN}}, \tag{D8}$$

denoting the strength of *cis*-inhibition. The dimensionless expressions of these terms are

$$\dot{x}_i = \ldots - \kappa_X^{\mathrm{cis}} x_i n_i, \tag{D9}$$

$$\dot{n}_i = \ldots - \kappa_X^{\mathrm{cis}} x_i n_i, \tag{D10}$$

following Eqs. (B1)–(B3), where we introduced

$$\kappa_X^{\mathrm{cis}} \equiv \frac{k_{XN}^{\mathrm{cis}} H_0}{d_h}.$$

APPENDIX E: DYNAMICS OF THE COMPLEX DeltaD: NOTCH EXTRACELLULAR DOMAIN

Here we introduce a variant of the model to consider the effects of internalized ligands on the dynamics of total DeltaD concentration. Upon binding of the ligands to Notch, the NICD is released in the signal-receiving cell i, and its dynamics is described by the variable S_i. Similarly to previous works [84,99,100], we have assumed that the remaining Notch extracellular domain (NECD), bound to a Delta ligand, is internalized in the signal-sending cell and effectively removed from the system. Since the Delta:NECD complex does not play a role in signaling, we have not considered its dynamics in the model so far. However, when accounting for the total DeltaD in the system, the dynamics of the complex should be included.

We modify Eq. (A29) to include the formation of the complex,

$$\mathrm{X}_i + \mathrm{N}_j \xrightarrow{\mathrm{k_{NX}}} \mathrm{W}_{Xi} + \mathrm{S}_j, \quad \mathrm{X} = \mathrm{C,D,E,F,G}, \tag{E1}$$

where W_{Xi} is the concentration of the complex formed by the ligand X and the NECD in cell i. After the complex is internalized, we assume that it is degraded [75,84,86] at the same rate d_W for any ligand X, so the dynamics are

$$\dot{W}_{Xi} = -d_W W_{Xi} + k_{NX} X_i \bar{N}. \tag{E2}$$

The dimensionless formulation of Eq. (E2) is given by Eqs. [(B1)–(B3)] and by defining

$$\delta_W \equiv \frac{d_W}{d_H},$$

such that

$$\dot{w}_{Xi} = -\delta_W w_{Xi} + \kappa_X x_i \bar{n}, \tag{E3}$$

for each $X = C, D, E, F, G$. These equations function as readouts from the model, since they do not feed back into the dynamics. Therefore, the dynamics of w_{Xi} can be obtained from the dynamics of the rest of the system Eqs. (B4)–(B11)

by exact integration of Eq. (E3). By means of an integrating factor

$$e^{\int \delta_W dt} = e^{\delta_W t}, \tag{E4}$$

we obtain

$$w_{Xi}(t) = e^{-\delta_W t} \int_0^t \kappa_X x_i(t') \bar{n}(t') e^{\delta_W t'} dt'. \tag{E5}$$

Including the internalized complexes, the total DeltaD in a cell is now given by

$$d_T(t) = d(t) + e(t) + 2g(t) + w_D(t) + w_E(t) + 2w_G(t), \tag{E6}$$

where dimer and dimer complex concentrations are zero in the monomer scenario, and the DeltaD:NECD complex concentration w_D is zero in the dimer scenario.

An alternative hypothesis to complex degradation is to assume that the ligand is recycled after activating Notch and being internalized [62]. In the limit where all the ligand is instantly recycled, the reaction in Eq. (A29) becomes

$$\mathrm{X}_i + \mathrm{N}_j \xrightarrow{\mathrm{k_{NX}}} \mathrm{X}_i + \mathrm{S}_j, \quad \mathrm{X} = \mathrm{C,D,E,F,G}, \tag{E7}$$

which amounts to removing loss terms of the form $-\kappa_X x_i \bar{n}$ form Eqs. (B5)–(B9).

APPENDIX F: METHODS

1. Numerical integration

We integrate the delayed differential equations (DDE) of the model numerically using a custom code that relies on the Python library `jitcdde` [127]. The library implements the Shampine-Thompson algorithm using adaptive time steps [128], and casts the DDEs Python code into compiled C code for faster execution. The initial condition for DDEs consists of the past history, up to the largest delay into the past. We set all variables in each cell to a constant value in the time interval $[-\tau, 0]$. To construct steady-state maps, for each cell we choose a random value from a uniform distribution in the range $[2, 6]$, which initialises the system in a desynchronized state. In desynchronization assays, we choose values in the range $[0, 0.01]$ to initialize the system in a synchronized state. We then evolve the model for a time roughly equivalent to 100 full cycles for steady-state assays and for 30 cycles in desynchronization assays. For a delayed negative feedback genetic oscillator, a first-order estimate of the cycle duration is $2(\tau + 1/d)$, where τ is the feedback delay and d the decay rate of h, that we use as timescale for nondimensionalizing the model equations [22,60,61]. We performed all numerical assays using $N_c = 100$ cells.

2. Synchronization

To quantify synchronization level of a population of genetic oscillators, we first obtain a phase $\theta_i(t)$ from the time series $h_i(t)$ using a numerical Hilbert transform [129], as implemented in the Python package Scipy [130]. We then compute the Kuramoto order parameter $R(t)$, defined as the modulus of the average of the complex phases of individual oscillations [69], $R(t)e^{i\varphi(t)} = N_c^{-1} \sum_{j=1}^{N_c} e^{i\theta_j(t)}$, where $\varphi(t)$ is the collective phase. The order parameter R is close to 1 when all phases θ_i stay close to the collective phase and drops to low values when they are spread out. Synchrony is therefore represented by a value close to 1. To quantify steady-state synchrony we take the temporal average $\bar{R} = \langle R(t) \rangle_t$ over a time window of about 80 steady-state cycles, ignoring the first 20 cycles to let transients elapse. This is the magnitude we report in synchronization maps.

3. ALD calculation

To measure the mean ALD of each mutant condition we perform 100 desynchronizaiton assays as described above. From each run we obtain $R(t)$ and the phase of the mean field from the Hilbert transform. Then, from the value of the phase at the time point where $R(t)$ crosses the threshold R_T we determine how many cycles the individual realization performed before the crossing. Since cells in the embryo go through a few cycles before the onset of somitogenesis [14], we allow for two initial cycles before starting the segment count.

[1] F. Marks, U. Klingmüller, and K. Müller-Decker, *Cellular Signal Processing: An Introduction to the Molecular Mechanisms of Signal Transduction* (Garland Science, New York, 2017).

[2] B. Alberts, *Molecular Biology of the Cell* (Garland Science, New York, 2017).

[3] L. Wolpert, C. Tickle, and A. M. Arias, *Principles of Development* (Oxford University Press, Oxford, 2015).

[4] E. R. Andersson, R. Sandberg, and U. Lendahl, Development **138**, 3593 (2011).

[5] K. G. Guruharsha, M. W. Kankel, and S. Artavanis-Tsakonas, Nat. Rev. Genet. **13**, 654 (2012).

[6] D. Henrique and F. Schweisguth, Development **146**, dev172148 (2019).

[7] N. Sachan, V. Sharma, M. Mutsuddi, and A. Mukherjee, FEBS J. **291**, 3030 (2023).

[8] A. C. Oates, L. G. Morelli, and S. Ares, Development **139**, 625 (2012).

[9] H. Shimojo and R. Kageyama, Semin. Cell Dev. Biol. **49**, 76 (2016).

[10] O. Pourquié, Dev. Biol. **485**, 24 (2022).

[11] O. F. Venzin and A. C. Oates, Dev. Biol. **460**, 40 (2020).

[12] Y.-J. Jiang, B. L. Aerne, L. Smithers, C. Haddon, D. Ish-Horowicz, and J. Lewis, Nature (London) **408**, 475 (2000).

[13] K. Horikawa, K. Ishimatsu, E. Yoshimoto, S. Kondo, and H. Takeda, Nature (London) **441**, 719 (2006).

[14] I. H. Riedel-Kruse, C. Müller, and A. C. Oates, Science **317**, 1911 (2007).

[15] E. A. Delaune, P. François, N. P. Shih, and S. L. Amacher, Dev. Cell **23**, 995 (2012).

[16] Y. Okubo, T. Sugawara, N. Abe-Koduka, J. Kanno, A. Kimura, and Y. Saga, Nat. Commun. **3**, 1141 (2012).

[17] A. Isomura, F. Ogushi, H. Kori, and R. Kageyama, Genes Dev. **31**, 524 (2017).

[18] K. Yoshioka-Kobayashi, M. Matsumiya, Y. Niino, A. Isomura, H. Kori, A. Miyawaki, and R. Kageyama, Nature (London) **580**, 119 (2020).

[19] Y. Yamanaka, S. Hamidi, K. Yoshioka-Kobayashi, S. Munira, K. Sunadome, Y. Zhang, Y. Kurokawa, R. Ericsson, A. Mieda, J. L. Thompson, J. Kerwin, S. Lisgo, T. Yamamoto, N. Moris, A. Martinez-Arias, T. Tsujimura, and C. Alev, Nature (London) **614**, 509 (2023).

[20] A. J. Krol, D. Roellig, M.-L. Dequéant, O. Tassy, E. Glynn, G. Hattem, A. Mushegian, A. C. Oates, and O. Pourquié, Development **138**, 2783 (2011).

[21] A. B. Webb, I. M. Lengyel, D. J. Jörg, G. Valentin, F. Jülicher, L. G. Morelli, and A. C. Oates, eLife **5**, e08438 (2016).

[22] J. Lewis, Curr. Biol. **13**, 1398 (2003).

[23] N. A. M. Monk, Curr. Biol. **13**, 1409 (2003).

[24] M. Jensen, K. Sneppen, and G. Tiana, FEBS Lett. **541**, 176 (2003).

[25] C. Schröter, S. Ares, L. G. Morelli, A. Isakova, K. Hens, D. Soroldoni, M. Gajewski, F. Jülicher, S. J. Maerkl, B. Deplancke, and A. C. Oates, PLoS Biol. **10**, e1001364 (2012).

[26] A. Trofka, J. Schwendinger-Schreck, T. Brend, W. Pontius, T. Emonet, and S. A. Holley, Development **139**, 940 (2012).

[27] F. J. M. van Eeden, M. Granato, U. Schach, M. Brand, M. Furutani-Seiki, P. Haffter, M. Hammerschmidt, C.-P. Heisenberg, Y.-J. Jiang, D. A. K. Robert, N. Kelsh, M. C. Mullins, J. Odenthal, R. M. Warga, M. L. Allende, E. S. Weinberg, and C. Nüsslein-Volhard, Development **123**, 153 (1996).

[28] S. A. Holley, D. Jülich, G.-J. Rauch, R. Geisler, and C. Nüsslein-Volhard, Development **129**, 1175 (2002).

[29] D. Jülich, C. Hwee Lim, J. Round, C. Nicolaije, J. Schroeder, A. Davies, R. Geisler, J. Lewis, Y.-J. Jiang, and S. A. Holley, Dev. Biol. **286**, 391 (2005).

[30] O. F. Venzin, C. Jollivet, N. Chiaruttini, O. Rosspopoff, C. Helsens, L. G. Morelli, K. Uriu, and A. C. Oates, bioRxiv (2023).

[31] S. A. Holley, R. Geisler, and C. Nüsslein-Volhard, Genes Dev. **14**, 1678 (2000).

[32] A. C. Oates and R. K. Ho, Development **129**, 2929 (2002).

[33] A. C. Oates, C. Mueller, and R. K. Ho, Dev. Biol. **280**, 133 (2005).

[34] G. J. Wright, F. Giudicelli, C. Soza-Ried, A. Hanisch, L. Ariza-McNaughton, and J. Lewis, Development **138**, 2947 (2011).

[35] B.-K. Liao, D. J. Jörg, and A. C. Oates, Nat. Commun. **7**, 11861 (2016).

[36] S. Hans and J. A. Campos-Ortega, Development **129**, 4773 (2002).

[37] L. G. Morelli, S. Ares, L. Herrgen, C. Schröter, F. Jülicher, and A. C. Oates, HFSP J. **3**, 55 (2009).

[38] L. Herrgen, S. Ares, L. G. Morelli, C. Schröter, F. Jülicher, and A. C. Oates, Curr. Biol. **20**, 1244 (2010).

[39] S. Ares, L. G. Morelli, D. J. Jörg, A. C. Oates, and F. Jülicher, Phys. Rev. Lett. **108**, 204101 (2012).

[40] K. Uriu, Y. Morishita, and Y. Iwasa, Proc. Natl. Acad. Sci. USA **107**, 4979 (2010).

[41] K. Uriu, S. Ares, A. C. Oates, and L. G. Morelli, Phys. Rev. E **87**, 032911 (2013).

[42] P. J. Murray, P. K. Maini, and R. E. Baker, Dev. Biol. **373**, 407 (2013).

[43] G. Roth, G. Misailidis, M. Pappa, J. Ferralli, and C. D. Tsiairis, Dev. Cell **58**, 967 (2023).

[44] C. Ho, L. Jutras-Dubé, M. Zhao, G. Mönke, I. Z. Kiss, P. François, and A. Aulehla, Proc. Natl. Acad. Sci. USA **121**, e2401604121 (2024).

[45] B. Pfeuty, J. Theor. Biol. **539**, 111060 (2022).

[46] D. J. Jörg, L. G. Morelli, and F. Jülicher, Phys. Rev. E **97**, 032409 (2018).

[47] A. Hubaud, I. Regev, L. Mahadevan, and O. Pourquié, Cell **171**, 668 (2017).

[48] Y. Ma and K. Yoshikawa, Phys. Rev. E **79**, 046217 (2009).

[49] Y. Masamizu, T. Ohtsuka, Y. Takashima, H. Nagahara, Y. Takenaka, K. Yoshikawa, H. Okamura, and R. Kageyama, Proc. Natl. Acad. Sci. USA **103**, 1313 (2006).

[50] K. Uriu, Y. Morishita, and Y. Iwasa, J. Math. Biol. **61**, 207 (2010).

[51] A. Ay, S. Knierer, A. Sperlea, J. Holland, and E. M. Özbudak, Development **140**, 3244 (2013).

[52] H. B. Tiedemann, E. Schneltzer, S. Zeiser, W. Wurst, J. Beckers, G. K. H. Przemeck, and M. H. d. Angelis, PLoS Comput. Biol. **10**, e1003843 (2014).

[53] O. Cinquin, J. Theor. Biol. **224**, 459 (2003).

[54] K. Uriu, Y. Morishita, and Y. Iwasa, J. Theor. Biol. **257**, 385 (2009).

[55] A. Ay, J. Holland, A. Sperlea, G. S. Devakanmalai, S. Knierer, S. Sangervasi, A. Stevenson, and E. M. Özbudak, Development **141**, 4158 (2014).

[56] H. Momiji and N. A. M. Monk, Phys. Rev. E **80**, 021930 (2009).

[57] Y. Bessho, R. Sakata, S. Komatsu, K. Shiota, S. Yamada, and R. Kageyama, Genes Dev. **15**, 2642 (2001).

[58] C. A. Henry, M. K. Urban, K. K. Dill, J. P. Merlie, M. F. Page, C. B. Kimmel, and S. L. Amacher, Development **129**, 3693 (2002).

[59] Y. Bessho, H. Hirata, Y. Masamizu, and R. Kageyama, Genes Dev. **17**, 1451 (2003).

[60] L. G. Morelli and F. Jülicher, Phys. Rev. Lett. **98**, 228101 (2007).

[61] B. Novák and J. J. Tyson, Nat. Rev. Mol. Cell Biol. **9**, 981 (2008).

[62] M. X. G. Ilagan and R. Kopan, Cell **128**, 1246 (2007).

[63] D. Soroldoni, D. J. Jörg, L. G. Morelli, D. L. Richmond, J. Schindelin, F. Jülicher, and A. C. Oates, Science **345**, 222 (2014).

[64] A. Mara, J. Schroeder, C. Chalouni, and S. A. Holley, Nat. Cell Biol. **9**, 523 (2007).

[65] K. Uriu, R. Bhavna, A. C. Oates, and L. G. Morelli, Biol. Open **6**, 1235 (2017).

[66] T. Fulton, B. Verd, and B. Steventon, R. Soc. Open Sci. **9**, 211293 (2022).

[67] G. Petrungaro, L. G. Morelli, and K. Uriu, Semin. Cell Dev. Biol. **93**, 26 (2019).

[68] See Supplemental Material at http://link.aps.org/supplemental/10.1103/7g6x-b238 for Supplemental Figs. S1–S7 and Supplemental Table S1.

[69] S. H. Strogatz, Physica D **143**, 1 (2000).

[70] P. Dornseifer, C. Takke, and J. A. Campos-Ortega, Mech. Dev. **63**, 159 (1997).

[71] J. Westin and M. Lardelli, Dev. Genes Evol. **207**, 51 (1997).
[72] S. Artavanis-Tsakonas, M. D. Rand, and R. J. Lake, Science **284**, 770 (1999).
[73] R. Kopan and M. X. G. Ilagan, Cell **137**, 216 (2009).
[74] D. Chen, Z. Forghany, X. Liu, H. Wang, R. M. H. Merks, and D. A. Baker, PLoS Comput. Biol. **19**, e1010169 (2023).
[75] K. Hori, A. Sen, and S. Artavanis-Tsakonas, J. Cell Sci. **126**, 2135 (2013).
[76] E. Ladi, J. T. Nichols, W. Ge, A. Miyamoto, C. Yao, L.-T. Yang, J. Boulter, Y. E. Sun, C. Kintner, and G. Weinmaster, J. Cell Biol. **170**, 983 (2005).
[77] K. Serth, K. Schuster-Gossler, E. Kremmer, B. Hansen, B. Marohn-Köhn, and A. Gossler, PLoS ONE **10**, e0123776 (2015).
[78] M. S. Bochter, D. Servello, S. Kakuda, R. D'Amico, M. F. Ebetino, R. S. Haltiwanger, and S. E. Cole, Dev. Biol. **487**, 42 (2022).
[79] The Alliance of Genome Resources Consortium, Nucleic Acids Res. **48**, D650 (2020).
[80] D. G. Howe, Y. M. Bradford, T. Conlin *et al.*, Nucleic Acids Res. **41**, D854 (2013).
[81] H. Mi, A. Muruganujan, D. Ebert, X. Huang, and P. D. Thomas, Nucleic Acids Res. **47**, D419 (2019).
[82] R. A. Bone, C. S. L. Bailey, G. Wiedermann, Z. Ferjentsik, P. L. Appleton, P. J. Murray, M. Maroto, and J. K. Dale, Development **141**, 4806 (2014).
[83] M.-L. Dequéant, E. Glynn, K. Gaudenz, M. Wahl, J. Chen, A. Mushegian, and O. Pourquié, Science **314**, 1595 (2006).
[84] D. Sprinzak, A. Lakhanpal, L. LeBon, L. A. Santat, M. E. Fontes, G. A. Anderson, J. Garcia-Ojalvo, and M. B. Elowitz, Nature (London) **465**, 86 (2010).
[85] D. Sprinzak, A. Lakhanpal, L. LeBon, J. Garcia-Ojalvo, and M. B. Elowitz, PLoS Comput. Biol. **7**, e1002069 (2011).
[86] M. Matsuda and A. B. Chitnis, Development **136**, 197 (2009).
[87] D. Chen, X. Liu, H. Wang, R. M. H. Merks, and D. A. Baker, PLoS Comput. Biol. **21**, e1012825 (2025).
[88] Y. Sun, H. Wallrabe, S.-A. Seo, and A. Periasamy, ChemPhysChem **12**, 462 (2011).
[89] M. A. Digman, R. Dalal, A. F. Horwitz, and E. Gratton, Biophys. J. **94**, 2320 (2008).
[90] L. Morsut, K. T. Roybal, X. Xiong, R. M. Gordley, S. M. Coyle, M. Thomson, and W. A. Lim, Cell **164**, 780 (2016).
[91] S. Toda, W. L. McKeithan, T. J. Hakkinen, P. Lopez, O. D. Klein, and W. A. Lim, Science **370**, 327 (2020).
[92] M. Matsuda, M. Koga, K. Woltjen, E. Nishida, and M. Ebisuya, Nat. Commun. **6**, 6195 (2015).
[93] C. Schröter, L. Herrgen, A. Cardona, G. J. Brouhard, B. Feldman, and A. C. Oates, Dev. Dynam. **237**, 545 (2008).
[94] J. Parres-Gold, M. Levine, B. Emert, A. Stuart, and M. B. Elowitz, Cell **188**, 1984 (2025).
[95] E. E. Alpay, O. Q. H. Zinani, X. Hu, A. Ay, and E. M. Özbudak, Nat. Commun. **16**, 2413 (2025).
[96] L. A. Rohde, A. Bercowsky-Rama, G. Valentin, S. R. Naganathan, R. A. Desai, P. Strnad, D. Soroldoni, and A. C. Oates, eLife **13**, RP93764 (2024).
[97] S. Okigawa, T. Mizoguchi, M. Okano, H. Tanaka, M. Isoda, Y.-J. Jiang, M. Suster, S.-i. Higashijima, K. Kawakami, and M. Itoh, Dev. Biol. **391**, 196 (2014).
[98] A. A. Granados, N. Kanrar, and M. B. Elowitz, Cell Genom. **4**, 100463 (2024).
[99] M. Boareto, M. K. Jolly, M. Lu, J. N. Onuchic, C. Clementi, and E. Ben-Jacob, Proc. Natl. Acad. Sci. USA **112**, E402 (2015).
[100] M. Boareto, M. K. Jolly, A. Goldman, M. Pietilä, S. A. Mani, S. Sengupta, E. Ben-Jacob, H. Levine, and J. N. Onuchic, J. R. Soc. Interface **13**, 20151106 (2016).
[101] M. K. Jolly, M. Boareto, M. Lu, J. N. Onuchic, C. Clementi, and E. Ben-Jacob, New J. Phys. **17**, 055021 (2015).
[102] J. C. Luna-Escalante, P. Formosa-Jordan, and M. Ibañes, Development **145**, dev154807 (2018).
[103] R. Kuintzle, L. A. Santat, and M. B. Elowitz, eLife **12**, RP91422 (2023).
[104] P. Formosa-Jordan and M. Ibañes, PLoS ONE **9**, e95744 (2014).
[105] J. C. Aster, W. S. Pear, and S. C. Blacklow, Annu. Rev. Pathol.: Mech. Dis. **12**, 245 (2017).
[106] H. Shimojo, T. Ohtsuka, and R. Kageyama, Neuron **58**, 52 (2008).
[107] R. Zhang, A. Engler, and V. Taylor, Cell Tissue Res. **371**, 73 (2018).
[108] P. A. Seymour, C. A. Collin, A. l. R. Egeskov-Madsen, M. C. Jørgensen, H. Shimojo, I. Imayoshi, K. H. de Lichtenberg, R. Kopan, R. Kageyama, and P. Serup, Dev. Cell **52**, 731 (2020).
[109] A. P. Jadhav, S.-H. Cho, and C. L. Cepko, Proc. Natl. Acad. Sci. USA **103**, 18998 (2006).
[110] E. A. Mills and D. Goldman, Curr. Pathobiol. Rep. **5**, 323 (2017).
[111] P. Formosa-Jordan, M. Ibañes, S. Ares, and J. M. Frade, Development **139**, 2321 (2012).
[112] D. Blanco-Obregon, M. J. Katz, L. Durrieu, L. Gándara, and P. Wappner, Dev. Biol. **462**, 101 (2020).
[113] J. Gao, L. Fan, L. Zhao, and Y. Su, Cell Regener. **10**, 11 (2021).
[114] L. Mancini, B. Guirao, S. Ortica, M. Labusch, F. Cheysson, V. Bonnet, M. S. Phan, S. Herbert, P. Mahou, E. Menant, S. Bedu, J.-Y. Tinevez, C. Baroud, E. Beaurepaire, Y. Bellaiche, L. Bally-Cuif, and N. Dray, Sci. Adv. **9**, eadg7519 (2023).
[115] S. C. van den Brink, A. Alemany, V. van Batenburg, N. Moris, M. Blotenburg, J. Vivié, P. Baillie-Johnson, J. Nichols, K. F. Sonnen, A. Martinez Arias, and A. van Oudenaarden, Nature (London) **582**, 405 (2020).
[116] N. Moris, K. Anlas, S. C. van den Brink, A. Alemany, J. Schröder, S. Ghimire, T. Balayo, A. van Oudenaarden, and A. Martinez Arias, Nature (London) **582**, 410 (2020).
[117] M. Hofer and M. P. Lutolf, Nat. Rev. Mater. **6**, 402 (2021).
[118] A. M. Arias, Y. Marikawa, and N. Moris, Dev. Biol. **488**, 35 (2022).
[119] I. M. Lengyel, D. Soroldoni, A. C. Oates, and L. G. Morelli, Papers Phys. **6**, 060012 (2014).
[120] I. M. Lengyel and L. G. Morelli, Phys. Rev. E **95**, 042412 (2017).
[121] G. A. Enciso, in *Nonautonomous Dynamical Systems in the Life Sciences*, edited by P. E. Kloeden and C. Pötzsche (Springer International, Cham, 2013), pp. 199–224.
[122] E. M. Özbudak and J. Lewis, PLoS Genet. **4**, e15 (2008).
[123] M. C. Mackey and L. Glass, Science **197**, 287 (1977).
[124] N. MacDonald, in *Time Lags in Biological Models*, edited by N. MacDonald (Springer, Berlin, 1978), pp. 1–12.
[125] A. Hanisch, M. V. Holder, S. Choorapoikayil, M. Gajewski, E. M. Özbudak, and J. Lewis, Development **140**, 444 (2013).

[126] H. G. Schuster and P. Wagner, Prog. Theor. Phys. **81**, 939 (1989).
[127] G. Ansmann, Chaos **28**, 043116 (2018).
[128] L. Shampine and S. Thompson, Appl. Numer. Math. **37**, 441 (2001).
[129] A. Pikovsky, M. Rosenblum, and J. Kurths, *Synchronization: A Universal Concept in Nonlinear Sciences* (Cambridge University Press, Cambridge, UK, 2001).
[130] P. Vijaykumar *et al.*, Nat. Methods **17**, 261 (2020).